Received: 30 January 2024 | Revised: 6 August 2024 | Accepted: 10 September 2024

DOI: 10.1002/jev2.12522

RESEARCH ARTICLE

Small RNAs in plasma extracellular vesicles define biomarkers of premanifest changes in Huntington's disease

Marina Herrero-Lorenzo[1] | **Jesús Pérez-Pérez**[2,3,4] | **Georgia Escaramís**[1,5] | **Saül Martínez-Horta**[2,3,4] | **Rocío Pérez-González**[2,3,4,6] | **Elisa Rivas-Asensio**[2,3,4] | **Jaime Kulisevsky**[2,3,4] | **Ana Gámez-Valero**[1,5] | **Eulàlia Martí**[1,5,7]

[1]Department of Biomedicine, Faculty of Medicine, Institute of Neurosciences, University of Barcelona, Barcelona, Catalunya, Spain

[2]Movement Disorders Unit, Neurology Department, Sant Pau Hospital, Barcelona, Catalunya, Spain

[3]Biomedical Research Institute (IIB-Sant Pau), Barcelona, Catalunya, Spain

[4]Center for Networked Biomedical Research in Neurodegenerative Diseases (CIBERNED), Madrid, Spain

[5]Biomedical Research Networking Center for Epidemiology and Public Health (CIBERESP), Spanish Ministry of Science and Innovation, Madrid, Spain

[6]Alicante Institute for Health and Biomedical Research (ISABIAL) and Neuroscience Institute, Alicante, Spain

[7]August Pi i Sunyer Biomedical research Institute (IDIBAPS), Barcelona, Catalunya, Spain

Correspondence
Ana Gámez-Valero and Eulàlia Martí, Department of Biomedicine, Faculty of Medicine, Institute of Neurosciences, University of Barcelona, C/ Casanova 143, Barcelona, 08036, Spain. Email: a.gamez@ub.edu and eulalia.marti@ub.edu

Funding information
Postdoctoral fellowship Juan de la Cierva, Grant/Award Number: FJC2019-039633-I; PhD Fellowship Spanish Ministry of Science and Innovation, Grant/Award Number: PRE2018-085617; Huntington's Disease Society of America (HDSA), Grant/Award Number: 2021 Human Biology Project; Spanish Ministry of Science and Innovation, Grant/Award Numbers: AEI/10.13039/501100011033, PID2020-113953RB-I00; Spanish Carlos III Health Institute (ISCIII), Grant/Award Numbers: PI17/01885, PI121/01758

Abstract

Despite the advances in the understanding of Huntington's disease (HD), there is a need for molecular biomarkers to categorize mutation carriers during the preclinical stage of the disease preceding functional decline. Small RNAs (sRNAs) are a promising source of biomarkers since their expression levels are highly sensitive to pathobiological processes. Here, using an optimized method for plasma extracellular vesicles (EVs) purification and an exhaustive analysis pipeline of sRNA sequencing data, we show that EV-sRNAs are downregulated early in mutation carriers and that this deregulation is associated with premanifest cognitive performance. Seven candidate sRNAs (tRF-Glu-CTC, tRF-Gly-GCC, miR-451a, miR-21-5p, miR-26a-5p, miR-27a-3p and let7a-5p) were validated in additional subjects, showing a significant diagnostic accuracy at premanifest stages. Of these, miR-21-5p was significantly decreased over time in a longitudinal study; and miR-21-5p and miR-26a-5p levels correlated with cognitive changes in the premanifest cohort. In summary, the present results suggest that deregulated plasma EV-sRNAs define an early biosignature in mutation carriers with specific species highlighting the progression and cognitive changes occurring at the premanifest stage.

KEYWORDS
biomarker, extracellular vesicles, Huntington's disease, miRNA, premanifest, small RNA, tRF

1 | INTRODUCTION

Huntington's disease (HD) is a dominantly inherited neurodegenerative disorder caused by a CAG triplet repeat expansion in the Huntingtin gene (*HTT*) (MacDonald et al., 1993). The main neuropathological hallmarks of HD are the presence of cytoplasmatic mutant HTT aggregates, the massive loss of the medium spiny neurons of the striatum, and cortical degeneration (Weir et al., 2011). In current clinical practice, manifest HD (M-HD) patients are diagnosed based on the appearance of a complex constellation of clinical symptoms, including progressive motor abnormalities, neuropsychiatric disturbances, early cognitive deterioration and dementia, among others (Bates et al., 2015; Finkbeiner, 2011). However, genetic analysis allows the use of predictive testing to identify premanifest gene-mutation carriers (P-HD) who may exhibit progressive brain changes in specific imaging metrics and cognitive performance long before the estimated time to diagnosis (Paulsen et al., 2008; Scahill et al., 2020).

Current treatments for HD provide only symptomatic relief, and later results on clinical trials investigating disease-modifying therapies have not shown significant efficacy so far (Przybyl et al., 2021). The combination of predictive genetic testing with new early molecular biomarkers could help in improving the design of clinical trials for HD by selecting appropriate patient populations, stratifying patients for intervention, monitoring treatment response and improving trial efficiency.

Recent efforts have been invested in the definition of HD biofluid-based biomarkers. The most remarkable one is mutant HTT, which can be measured in the cerebrospinal fluid (CSF) to assess the efficacy of mutant HTT-lowering therapies (Wild et al., 2015). Further, it has been shown that minimally invasive plasma biomarkers can reflect molecular changes occurring in this heterogeneous disorder. Specifically, plasma neurofilament light chain (NfL) shows a higher prognostic value than mutant HTT (Rodrigues et al., 2020; Southwell et al., 2015), despite not being disease-specific, as it is also observed in other brain-related diseases (Tabrizi et al., 2019, 2020). Otherwise, regarding RNA-based biomarkers, microRNAs (miRNAs) have been largely studied as promising transcriptomic biomarkers since they are stable in peripheral circulation (Dong & Cong, 2021), and their levels are highly sensitive to physiological and pathological states (Leidinger et al., 2013; Sheinerman et al., 2012; Tan et al., 2014). Moreover, we have recently shown that not only miRNAs but other small RNAs (sRNAs, <200 nucleotides) may have a profound role in HD pathogenesis (Creus-Muncunill et al., 2021). The intrastriatal injection of sRNAs from HD patients' brains triggers motor abnormalities, neuronal toxicity and transcriptional alterations in naïve mice (Creus-Muncunill et al., 2021). These results suggest that different types of sRNAs are sufficient to induce neurotoxicity and are likely involved in the progressive transcriptomic deregulation underlying HD pathogenesis. Therefore, a better understanding of sRNA expression dynamics should provide clues about the progression of the disease and help to elucidate if sRNA perturbations are an early phenomenon in HD.

In peripheral circulation, extracellular sRNAs (exRNAs) can be found freely circulating, associated with lipid- or protein-complexes, or encapsulated within different types of vesicles. Specifically, extracellular vesicles (EVs) are bilayered vesicles secreted by many cell types that encapsulate molecules such as RNAs and proteins from the cell of origin, which makes them attractive in biomarker discovery (Fritz et al., 2016; Geekiyanage et al., 2020; Tosar et al., 2015; Vickers et al., 2011). Nevertheless, recent studies have raised controversy as they show that the vast majority of circulating exRNAs are not found in EVs, but co-purifying with other molecules in the extravesicular milieu (Arroyo et al., 2011; Tosar et al., 2020). In plasma, proteins such as Argonaute2 ribonucleic complexes have been described as important miRNA carriers (Arroyo et al., 2011); however, no solid evidence regarding the distribution of sRNA biotypes in the plasma subfractions has been described so far.

Herein, we aimed to define biomarkers to monitor changes that occur in the pre-symptomatic HD population, by exploring plasma sRNA levels. We analyzed sRNA profiles of EV-enriched and NonEV plasma fractions from P-HD and M-HD mutation carriers in comparison to control samples. Our data indicate that sRNA levels are less variable in EVs compared with NonEVs fractions and further suggest that most sRNAs are downregulated in EVs of mutation carriers, with many species altered at premanifest stages. Importantly, specific sRNAs showing altered expression over time correlate with the premanifest cognitive clinical score, which may lead to the definition of novel early progression biomarkers.

2 | METHODS

2.1 | Participants

In this study, all participants were recruited from the Movement Disorders Unit at Hospital de la Santa Creu i Sant Pau (Barcelona, Spain). We included 41 Caucasian gene mutation carriers and 22 Caucasian healthy non-mutation carrier control participants (Tables 1, 3 and S1). Individuals were confirmed gene mutation carriers (CAG repeat length > 40), and disease-specific indicators including motor, cognitive and neuropsychiatric status, were recorded.

The disease burden score (DBS) was used as an index of pathological burden due to lifetime exposure to mutant huntingtin and calculated as age (in years) × (CAG – 35.5). Gene-mutation carriers were grouped into premanifest (P-HD, $n = 21$) and manifest (M-HD, $n = 20$) stages based on the Unified Huntington's Disease Rating Scale total motor score (UHDRS-TMS) and the Total Functional Capacity (TFC). Participants were classified as M-HD patients if UHDRS-TMS > 5 and a diagnostic confidence

level = 4, indicating that motor abnormalities were unequivocally caused by HD with ≥99 % of confidence. Participants with a diagnostic confidence level (DCL) < 4 and a TFC = 13 were considered P-HD.

The following cognitive indicators, known to be sensitive to HD progression, were also administered: The Symbol Digit Modality Test (SDMT) and the Stroop-word reading test (SWRT) (Braisch et al., 2019; Sampedro et al., 2022). The Composite UHDRS (cUHDRS) score was also calculated (Schobel et al., 2017).

All participants provided written informed consent previously approved by the appropriate ethics committee. The study was therefore performed in accordance with the ethical standards laid down in the 1964 Declaration of Helsinki and its later amendments.

2.2 | Sample collection and processing

Blood samples were collected in tubes with 0.109 M 3.2% trisodium citrate (Vacutainer, Becton Dickinson) via antecubital vein puncture in the morning, and processed within 30 min after withdrawal. Tubes were centrifuged at 500 *g* for 10 min at room temperature (RT) and the supernatant was pipetted off from cell debris. The supernatant was centrifuged again at 2500 *g* for 15 min at RT to eliminate platelets and one more time at 13,000 *g* for 15 min at RT to eliminate bigger particles and smaller aggregates. Platelet-free plasma was collected and stored directly at −80°C.

2.3 | Plasma NfL

NfL was measured with the Simoa Human NF-light Advantage kit (Catalogue # 103400) using the Single Molecule Array (Simoa) technology (Simoa; Quanterix, Lexington, MA, United States) in the SR-X Biomarker detection system by following the manufacturer's instructions. Briefly, the calibration curve, control samples, inter-assay control (pooled plasma with known concentration) and unknown samples in duplicate were loaded onto a 96-well plate. Samples were incubated with antibody-coated paramagnetic beads and a biotinylated antibody detector simultaneously. After a wash, streptavidin-conjugated β-galactosidase (SBG) reagent was added to bind the biotinylated antibodies, leading to the SBG enzyme labelling of the capture of NfL. Once in the SR-X platform, the beads were resuspended in resorufin β-D-galactopyranoside (RGP) reagent, transferred to the Simoa disk and sealed. The NfL proteins captured by the antibody-coated paramagnetic beads and labelled with the SBG reagent hydrolyze the RGP substrate to produce a fluorescent signal. The fluorescent signal values generated from the calibration curve of known concentrations were fit using a 4-parameter logistic curve that was used to calculate the unknown and control sample concentrations. All the samples were measured in duplicate and had an intra-assay coefficient of variation (CV) < 20% with a mean of 7.54%. Inter-assay CV% was 9.34%.

2.4 | Plasma fractionation and EVs isolation

For plasma fractionation and EVs isolation, we used size-exclusion chromatography (SEC) followed by ultrafiltration (UF) as previously described (Gámez-Valero et al., 2016; Gámez-Valero et al., 2019). Briefly, Sepharose CL-2B (Sigma–Aldrich, MO, USA) was stacked in Puriflash Dry-Load Columns (Interchim) of 20 mL. On top of each column, 2 mL of plasma were loaded, and fractions of 500 µL were collected manually in individual tubes (a total of 35 fractions) using filtered 1X PBS as elution buffer. Protein content for each fraction was measured by Micro BCA Protein Assay Kit (Thermo Fisher Scientific) and Bio-Rad Protein Assay Dye Reagent (BioRad). SEC-fractions were further characterized using classical EVs-associated markers CD9, CD63, and CD81 by bead-based flow cytometry assay as previously reported (Monguió-Tortajada et al., 2019). Briefly, 50 µL of each SEC-fraction or 50 µL of 1X PBS (as negative control) were incubated with aldehyde/sulphate latex, 4% w/v 4 µm beads (A37304, Invitrogen, Thermo Fisher Scientific) for 15 min at RT. For bead blocking, 1 mL of bead-coupling buffer (BCB; 1X PBS supplemented with 0.1% BSA and 0.01% sodium azide, both from Sigma) was added to each fraction and fractions were left overnight (O/N) on rotation. Beads were pelleted and washed by centrifugation at 2000 × *g* for 10 min. We removed the supernatant and resuspended the bead-coupled samples with 200 µL of BCB. Next, bead-coupled samples were labelled with 50 µL of anti-CD9 (mouse hybridoma, gifted), anti-CD63 (mouse hybridoma, gifted) and anti-CD81 (81PU-01MG) as primary antibodies for 30 min at 4°C. Negative control was incubated with isotype IgG (ab37355, Abcam) was added. Samples were washed with 150 µL of BCB centrifuging at 2000 × *g* for 10 min. Then, bead-coupled samples were incubated with FITC-conjugated secondary goat anti-human antibody (1032-02, Southern Biotech) for 30 min at 4°C. After washing with BCB, each sample was resuspended with 190 µL of 1X PBS. Samples were further analyzed in a BD LSRFortessa (BD Biosciences) using the FACSDiva Software. A total of 10,000 beads were acquired for each sample and the median fluorescence intensity (MFI) values were obtained. The MFI values were normalized relative to the negative control (fold change MFI). Finally, the four fractions with the highest MFI for the three markers were considered EVs-enriched fractions and were pooled. Purified pooled EVs were further concentrated by ultrafiltration using Amicon

Ultra 100 KDa Centrifugal Filters (Merck Millipore) according to the manufacturer's instructions, obtaining the concentrated EVs (cEV fraction) and Filtrate fractions (Figure 1a). Pooled fractions were kept at −80°C until later use.

For the determination of sRNA diversity in the different plasma subfractions, four SEC fractions depleted of EVs with low protein concentration (NonEVs-Low fraction) and four SEC fractions depleted of EVs with high protein content (NonEVs-High fraction) were also pooled (Figure 1b).

For the analysis of expression patterns of plasma sRNAs in the paradigm of HD, eight EV-depleted SEC fractions (identified as NonEVs fraction) were pooled to investigate the extravesicular fraction in the patients' and healthy controls' groups (Figure 2b).

2.5 | Nanoparticle tracking analysis

The particle size distribution and concentration measurements in cEVs fractions were evaluated by nanoparticle tracking analysis (NTA) using a NanoSight NS300 instrument (Malvern Panalytical) and following the manufacturer's instructions. Each sample was diluted in sterile and filtered 1X PBS to the working range of the system (106–109 particles/mL). Data acquisition and processing were performed using the Nanosight NS300 software (version 3.4) recording three 30-s videos with 25 frames per second. Camera type was sCMOS with Laser Type Blue488 and Camera Level 12. Video analysis settings were set to a detection threshold of 5.

2.6 | Western blotting

Assessment of specific EV markers and NonEV markers was performed by Western blotting. Protein concentration was measured by Micro BCA Protein Assay Kit (Thermo Fisher Scientific) in the cEVs and Filtrate fractions, samples with low input of protein. Protein concentration in NonEVs-Low fractions, NonEVs-High fractions, and cell lysate samples was determined using Bio-Rad Protein Assay Dye Reagent (BioRad). Equal protein amount of each sample (20 μg) was mixed with reducing 5X Pierce Lane Marker Reducing Sample Buffer (Thermo Fisher Scientific) and boiled for 5 min at 95°C. Due to their not-existing protein content, for Filtrate fractions, the same volume as the one corresponding to 20 μg of the cEVs fractions (from original sample), was loaded. Samples were resolved in NuPAGE 4%–12% Bis-Tris polyacrylamide gels (Thermo Fisher Scientific) using MOPS SDS as running buffer (Thermo Fisher Scientific). Gels were transferred to nitrocellulose membranes with the iBlot2 system (Thermo Fisher Scientific). In order to visualize the depletion of Albumin and IgGs in cEVs fractions, Ponceau S staining (Sigma–Aldrich) was applied. Membranes were blocked with 5% non-fat dry milk (sc-2325, Santa Cruz Biotech) diluted in 1X Tris-buffered saline with 0.1% Tween 20 (TBS-T) for 1 h at RT. Blots were incubated overnight at 4°C with the following primary antibodies: rabbit anti-CD9 (13174, Cell Signalling Technology), rabbit anti-Alix (12422-1-AP, Proteintech), mouse anti-Flotillin1 (610820, BD Biosciences), rabbit anti-TSG101 (ab30871, Abcam), rabbit anti-Syntenin (ab133267, Abcam), rabbit anti-Calnexin (ab22595, Abcam) or mouse anti-OxPhos Complex IV subunit IV (anti-COX IV; A-21347, Thermo Fisher Scientific) diluted 1:1000 in TBS-T with 5% Bovine Serum Albumin (BSA, Sigma). Membranes were then washed three times in TBS-T and incubated for 1 h at RT with goat anti-rabbit or goat anti-mouse HRP conjugated secondary antibodies (31460 and 31430, respectively, Thermo Fisher Scientific) diluted 1:10,000 in TBS-T. Blots were washed again three times in TBS-T and detected with SuperSignal West Pico Plus or SuperSignal West Femto Maximum Sensitivity chemiluminescent substrates (Thermo Fisher Scientific). Images were acquired in the imaging system Chemidoc (BioRad).

2.7 | Cryogenic transmission electron microscopy

Plasma subfractions were imaged by cryogenic transmission electron microscopy (cryo-EM). Vitrified specimens were prepared by placing 3 μL of a sample on a Quantifoil 1.2/1.3 TEM grid, blotted to a thin film and plunged into liquid ethane-nitrogen in the Leica EM-CPC cryo-work station. The grids were transferred to a 626 Gatan cryo-holder and maintained at −179°C. The grids were analyzed with a Jeol JEM 2011 transmission electron microscope operating at an accelerating voltage of 200 kV. Images were recorded on a Gatan Ultrascan 2000 cooled charge-coupled device (CCD) camera with the Digital Micrograph software package (Gatan). Size distribution of EVs was quantified using the ImageJ tool. Briefly, images of each sample were converted from pixel measurements to nanometers. The diameter of approximately 200 vesicles per sample was determined, approximately 80% of EVs exhibiting a size within the expected size range of 40–200 nm. The percentage of the total number of EVs with sizes between 0–40, 40–80, 80–120, 120–160, 160–200 and greater than 200 nm was calculated relative to the total number of EVs measured in each sample. The differences between groups were then compared.

2.8 | RNA extraction and small RNA sequencing

sRNA was isolated using the miRNeasy Serum/Plasma Advanced Kit (Qiagen) according to the manufacturer´s instructions. All samples were adjusted to an input final volume of 200 µL. RNA samples were eluted in 20 µL of RNAse-free water. Prior to sequencing, RNA was precipitated using glycogen (20 mg/mL, Roche), sodium acetate 3 M pH 4.8 (Sigma–Aldrich) and 100% ethanol. After 24 h at −20°C, the mixtures were centrifuged at 14,000 rpm for 30 min at 4°C. Carefully, the supernatant was removed, and the pellet was then washed with 75% ethanol followed by centrifugation at 12,000 rpm for 5 min at 4°C. Finally, the supernatant was discarded, and the RNA pellet was dried at RT and dissolved at 65°C for 3 min in 6 µL of RNAse-free water and stored keeping the cold chain at −80°C.

The RNA samples were subjected to quality and degradation analysis using the Bioanalyzer 2100 (Agilent), resulting in an RNA yield of approximately 50–100 pg/µL. sRNA libraries were generated using the NEBNext Small RNA Library Preparation Set for Illumina (New England Biolabs) following the manufacturer's instructions. Indexed libraries were equimolarly pooled, and the selected band of interest (145–160 bp) was purified. Single-end sequencing of libraries was then carried out on the Illumina HiSeq 2000 with read lengths of 50 nt, generating at least 8 million reads per sample.

sRNAseq raw data of all samples are available at GEO under accession number GSE273501.

2.9 | Bioinformatic and biostatistical analysis

The quality of the sequenced fastq files was checked using the FastQC software (http://www.bioinformatics.babraham.ac.uk/projects/fastqc/) and sequence quality scores across all bases of EVs and NonEVs fractions per group were obtained (Figure S1a). Adapter trimming was performed with Cutadapt (Martin, 2011) and the trimmed reads were aligned to the human genome (version Ensemble hg19) using STAR aligner (version 2.7.9a) (Dobin et al., 2013) (Figure S1b). The obtained sequences were annotated and quantified using SeqCluster (Pantano et al., 2011) and ExceRpt (NIH ExRNA Communication Consortium -ERCC-) (Rozowsky et al., 2019) bioinformatic tools. During the pre-processing step, ExceRpt filters out highly abundant sRNAs mapping onto ribosomal RNAs (rRNAs) and makes an oversimplification of the highly complex tRNA-derived fragments (tRFs) landscape by only considering the type of isoacceptor. Because non-randomly generated rRNA fragments and tRFs are bioactive molecules (Shi et al., 2021) that are emerging as appealing biomarkers (Thompson et al., 2008; Tosar & Cayota, 2020), we used SeqCluster tool to highlight these biotypes. SeqCluster uses a heuristic iterative algorithm to deal with multi-mapped events. Sequences are consistently and non-redundantly grouped if they map onto the same genomic site defining 'clusters' of co-expressed sRNAs. Clusters are then classified according to the type of precursor where sRNAs map, including rRNA-and tRF-clusters. We generated ExceRpt and SeqCluster count matrices with raw reads of each sRNA biotype in every sample. To detect outlier samples in the RNAseq analysis, we generated PCA plots with the normalized sRNAs sequence count matrix and we did not identify any outlier (Figure S1c).

Prior to further analyses, only sRNAs identified with a minimum of 10 counts in at least half of the samples of the tested conditions were considered. Differential expression analyses were performed through negative binomial generalized models implemented in the Bioconductor package DESeq2 (Love et al., 2014) from R statistical software. Age and sex were considered as confounding factors and Benjamini–Hochberg correction for multiple testing was applied to control the False Discovery Rate.

Partial least squares discriminant analysis (PLS-DA), a multivariate supervised classifier, was performed separately for miRNA, tRFs and gene fragments biotypes, following a highly strict refinement strategy as previously described (Pantano et al., 2016). In brief, a first PLS-DA was conducted for each sRNA biotype to separate P-HD vs CTL, M-HD vs CTL, and M-HD vs P-HD. sRNAs strongly contributing to the separation between groups were selected to perform a second PLS-DA. The Variable Importance for the Projection (VIP) criterion was used to consider the contribution of a specific sRNA. To ensure the Variable Importance of the final model, we selected sRNAs with VIP > 1.2 in the initial PLS-DA model to construct the second model. We then focused on the sRNAs with the highest contributions in the second PLS-DA analysis (sRNAs with VIP > 0.8). To assess validity and robustness of the method used, a permutation test was employed which involved 1,000 datasets, where class labels were randomly reassigned at each iteration. Significance was then calculated by assessing how many times the random reassignment of individuals to classes yields a result better than the original classification. Principal Component Analysis (PCA) was applied as a non-supervised method to evaluate the separation between disease conditions using the top contributing sRNAs based on the refined PLS-DA analysis. For both PLS-DA and PCA analyses count matrices normalized and transformed to variance-stabilized expression levels were used.

The determination coefficient (R^2) from partial least squares regression (PLSR) models was used to decipher which clinical parameter was better explained by the grouped top DE sRNAs. Permutation tests (1,000 permutations) were applied for statistical significance purposes. Correlation analyses between qPCR-validated sRNAs, NfL, and clinical data were performed using partial correlation test including age and sex as confounding factors.

A 5% statistical significance level was considered across all analyses.

2.10 | qRT-PCR validation

Half of the volume of EVs and NonEVs pooled fractions was used for RNA isolation as described in the section 'RNA extraction and small RNA sequencing' with minor modifications. Prior to RNA sample lysis using RPL buffer, synthetic RNA spike-ins (UniSp2, UniSp4, UniSp5 RNA Spike-in mix; Qiagen) were added and used as quality controls for RNA isolation, in accordance with the kit protocol. Two microliter of isolated RNA were used for reverse transcription (RT) and cDNA synthesis using the miRCURY LNA RT Kit (Qiagen) according to the manufacturer's instructions adding the RNA spike-in UniSp6 as quality control for RT. The obtained cDNA was further diluted 1:10 for qPCR and, 3 µL were used as template in a 10 µL final volume reaction using the miRCURY LNA SYBR Green PCR Kit (Qiagen) in a StepOnePlus Real-Time PCR System (Applied Biosystems). For miRNAs validation, specific LNA PCR primer assays (Qiagen) for hsa-miR-451a, hsa-miR-21-5p, hsa-miR-26a-5p, hsa-let-7a-5p, hsa-miR-27a-3p (YP02119305, YP00204230, YP00206023, YP00205727 and YP00206038, respectively) were used. For tRFs validation, custom LNA PCR primers were designed and synthesized by Qiagen for hsa-tRF-Glu-CTC (5′-TCCCTGGTGGTCTAGTGGTTAGGATTCGGCG-3′), hsa-tRF-Gly-GCC (5′-GCATTGGTGGTTCAGTGGTAGAATTCTCGC-3′) and hsa-tRF-Lys-TTT (5′-TAGCTCAGTTGGTAGAGC-3′). For each determination, reactions were performed in triplicate.

Due to the absence of universal endogenous sRNA normalizers in EVs, miR-100-5p was selected as the housekeeping gene since it was one of the most stable sRNAs in terms of least variability across all the sequenced samples and highly expressed. For the analysis of deregulation based on relative quantification (RQ) of qRT-PCR data, linear mixed-effects models (LMM) were applied that accounted for the different sources of variation derived from the experimental design. Age and sex were considered as confounding factors. For the longitudinal study of the selected sRNAs validated, sensitivity analysis was done before the comparison between longitudinal time-points. In this sense, control samples, P-HD mutation carriers at the baseline time-point and P-HD mutation carriers at the follow-up time-point were run in parallel. Progression of RQ values was evaluated with the LMM models, which accounted as well here for the correlation structure of the longitudinal nature data.

The diagnostic accuracy of validated sRNAs was explored by receiver operating characteristic (ROC) curves. For the analysis of sRNA biosignatures, logistic binary regression was applied, and the obtained estimated probabilities were used to build ROC curves. Area under the ROC curve (AUC) and its 95% confidence interval were used as the diagnostic accuracy metric.

2.11 | EV-TRACK

We have submitted all relevant data of our experiments to the EV-TRACK knowledgebase (Van Deun et al., 2017) (EV-TRACK ID: EV230044).

3 | RESULTS

3.1 | Different plasma subfractions show specific sRNA profiles

Aiming to understand exRNA distribution in plasma, we profiled sRNAs associated with different plasma subfractions. To this end five plasma samples from healthy volunteers were subfractionated through size-exclusion chromatography followed by ultrafiltration (SEC-UF) (Monguió-Tortajada et al., 2019) (Figure 1a). As described previously (Gámez-Valero et al., 2016; Gámez-Valero et al., 2019), SEC-eluted fractions enriched in EVs were determined by flow cytometry, and the four fractions showing positivity for tetraspanins CD9, CD63 and CD81 were pooled (Figure 1b). Subsequently, tetraspanins-positive pooled fractions were concentrated by UF obtaining a concentrated EVs-enriched fraction (cEVs) and an eluted fraction without EVs (Filtrate). In parallel, tetraspanins-negative SEC-eluted fractions showed an increasing protein concentration (NonEVs fractions) and we selected two different fractions: fractions with low concentration of protein (NonEVs-Low) and fractions showing the highest concentration of protein (NonEVs-High) (Figure 1a).

cEVs were further characterized as recommended in the MISEV guidelines (Théry et al., 2018). cEV particle concentration yielded $8.33 \times 10^9 \pm 2.65 \times 10^8$ particles/mL with a mean diameter size of 146.0 ± 2.8 nm as determined by NTA (Figure 1c). Western Blot was used to confirm the presence of additional EV markers in cEVs fractions and the absence of them in the UF filtrate, NonEVs-Low and NonEVs-High fractions, as well as the lack of cell markers for intracellular contamination (Figure 1d). The reduction of Albumin and other plasma abundant proteins in the cEVs fractions was confirmed by Ponceau red staining of the membrane (Figure S2a). Cryo-TEM images confirmed the expected size range and morphological features in cEV fractions, and absence of EVs in Filtrate, NonEVs-Low and NonEVs-High fractions (Figure 1e). Overall, this setup indicates that we have successfully obtained differentiated plasma subfractions with the potential to show specific sRNAs profiles.

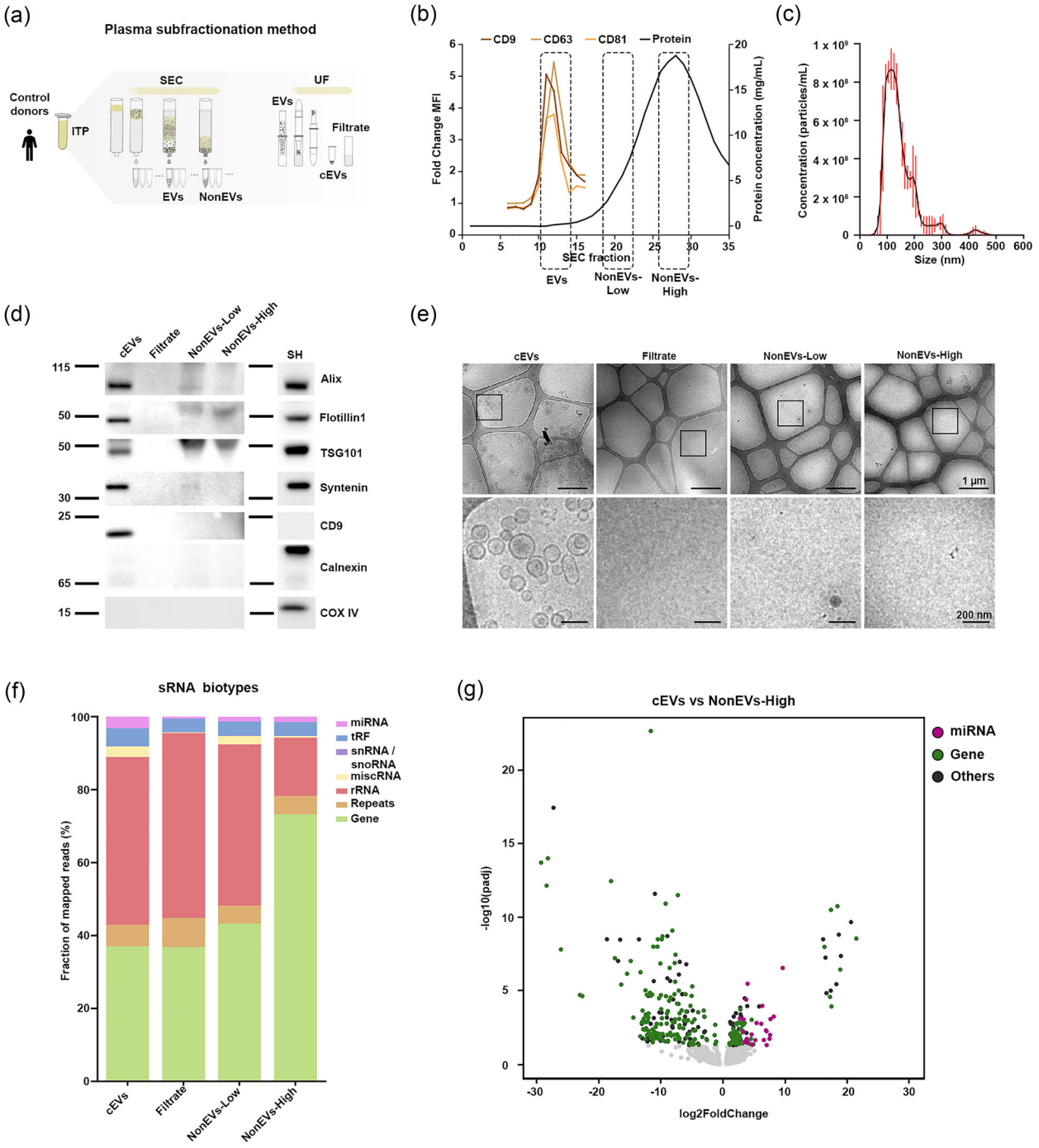

FIGURE 1 sRNA biotypes are differently distributed between plasma subfractions. (a) Schematic representation of plasma-EV isolation procedure by SEC and UF and selected fractions for analysis: cEVs, Filtrate, NonEVs-Low, and NonEVs-High fractions. (b) Representative SEC profile of plasma samples showing EV elution in low-protein fractions as measured by Bradford protein assay and enriched in CD9, CD63, and CD81 markers as analyzed by flow cytometry. (c) Representative NTA size distribution profile of cEVs fraction ($n = 5$). (d) Western Blot analysis of isolated fractions. Fractions were analyzed for the presence of EV markers (Alix, Flotillin1, TSG101, Syntenin and CD9) and negative EV-markers (Calnexin and COX IV). SH-SY5Y cell lysate (SH) was used as positive controls. (e) Representative images of cryo-EM of the isolated fractions. Upper images, bar = 1 µm. Lower images, bar = 200 nm. Using SeqCluster tool: (f) Fraction of reads that align to small RNA types are shown per plasma subfraction. Mean ± SD is shown. (g) Volcano plot showing differentially expressed sRNAs in cEVs versus NonEVs-High fractions. Pink dots represent DE miRNAs and green dots represent DE gene fragments. ($|\log2FoldChange| > 0.58$, adj $p < 0.05$). Samples of each subfraction, $n = 5$.

To uncover the sRNA diversity in the different plasma subfractions, we used SeqCluster (Pantano et al., 2011) and ExceRpt (Rozowsky et al., 2019) bioinformatic tools, offering complementary information (see Section 2). We detected heterogeneous proportions of sRNAs biotypes in the different plasma fractions, dominated by rRNA- and gene fragments (Figures 1f, S3a and S4a,b). The distribution of sRNA biotypes in the different fractions suggests an increased proportion of miRNAs in cEVs and an elevated proportion of gene fragments in NonEVs-High fractions (Figures 1f, S3a and S4a). Focusing on the total number of different sRNA biotypes identified in each subfraction, we observed that cEVs fractions contained an increased number of miRNAs (Figures S3b and S4c), while a similar diversity was detected for other species in the different subfractions (Figures S3b and S4c).

These observations were confirmed by applying DESeq2 differential expression (DE) analysis between EVs and NonEVs-High fractions, to highlight species differently enriched in these fractions. DE-miRNAs, a total of 26 (adjusted p; adj $p < 0.05$), were all more represented in cEVs, and most DE-gene fragments (139 out of 200) were enriched in the NonEVs-High fractions (Figures 1g and S4d). In line with these results, hierarchical clustering analysis based on miRNA levels showed that cEVs fractions grouped in a common cluster (Figure S3c and S4e). Similarly, NonEVs-High fractions were clustered when using the count matrix of sRNAs mapping onto genes (Figures S3d and S4f).

These findings suggest that both cEVs and NonEVs-High fractions show distinct patterns of sRNA and may provide complementary information.

3.2 | No major differences were found in plasma EV morphology and concentration between control and *HTT* mutation carriers

Once the general profiling of sRNA diversity in plasma subfractions was established, we next sought to analyze the expression pattern of plasma exRNAs in *HTT* mutation carriers. For this purpose, three different groups of samples were considered: P-HD, M-HD and healthy control volunteers (CTL) (Table 1, $n = 10$ samples per group). We then selected the two plasma fractions showing distinct sRNA patterns: the cEVs enriched fraction (EV) and the fraction depleted of cEVs showing a high protein concentration (NonEV) (Figure 2a). EVs were further characterized in a representative subset of samples based on MISEV guidelines (Théry et al., 2018) and compared between the three groups. Regarding tetraspanins expression, we did not observe any difference between groups (Figure 2b,c). Western Blot was used to confirm the presence of TSG101, Flotillin1 and Alix, and the absence of Calnexin and COX IV in representative EVs (Figure 2d). Moreover, Ponceau red staining in the two fractions suggested a strong reduction of highly abundant plasma proteins in cEV fractions (Figure S5a). Likewise, no statistical differences were observed in EVs concentration between groups as measured by NTA (Figure 2e); although a trend for an increased concentration in the M-HD group is observed, in line with an analogous trend in the tetraspanins levels (Figure 2c). The analysis of NTA concentrations divided by discrete sizes revealed significant differences in the size distribution between P-HD and M-HD in comparison to CTL samples. Specifically, an increase in vesicles ranging 80–120 nm and a decrease in vesicles > 200 nm (Figure S5b). Using cryo-EM, we confirmed the integrity of EVs (Figures 2f and S5c); however, we could not recapitulate the size differences between

TABLE 1 Clinic and sociodemographic characteristics of samples used for sRNA sequencing.

	Total	CTL	P-HD	M-HD
Age (years)	47.2 ± 12.55	45.2 ± 12.4	41.2 ± 7.9	55.5 ± 13.2
Sex (male/female)	11/19	4/6	3/7	4/6
CAG repeats	–	–	42.9 ± 2.02	42.40 ± 2.50
DBS[a]	–	–	294.80 ± 61.17	420.02 ± 152.67
cUHDRS[b]	–	17.44 ± 0.56	17.32 ± 1.62	8.73 ± 5.12
UHDRS-TMS[c]	–	0	0.6 ± 1.58	34.90 ± 29.3
TFC[d]	–	13 ± 0	12.90 ± 0.32	10.60 ± 2.27
SWRT[e]	–	105.75 ± 13.23	103.80 ± 21.32	56.60 ± 27.10
SDMT[f]	–	52.25 ± 8.77	53.00 ± 11.58	22.10 ± 16.33
Plasma NfL (pg/mL)	–	6.81 ± 1.74	21.03 ± 33.24	31.41 ± 14.35

[a]Disease Burden Score as measured by age × (CAG-35.5).
[b]Composite Unified Huntington Disease Rating Scale.
[c]Unified Huntington Disease Rating Scale–Total Motor Score.
[d]Total Functional Capacity.
[e]Stroop Word Reading Test.
[f]Symbol Digit Modality Test.

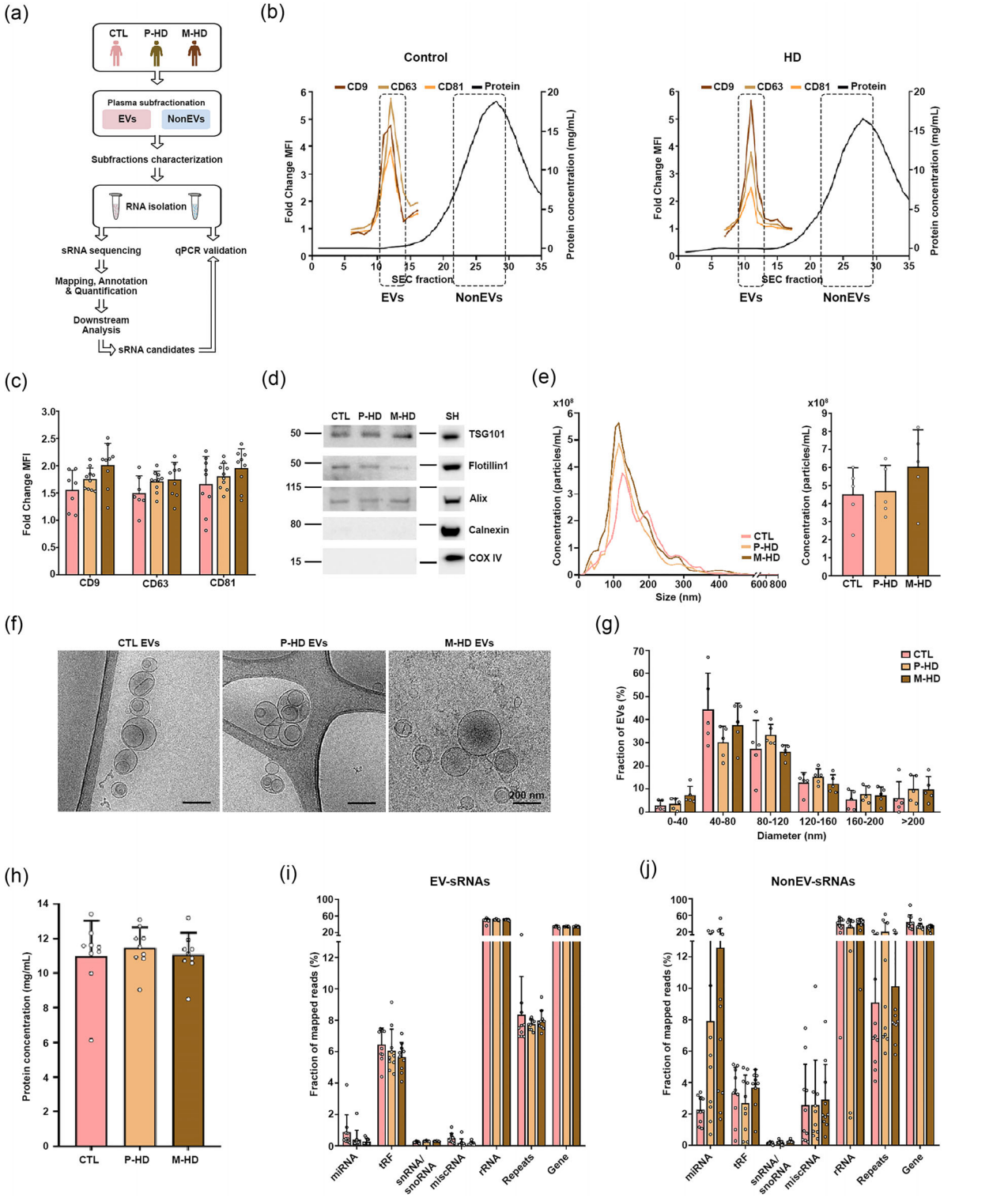

FIGURE 2 Characterization of EV fraction and NonEV fraction isolated from P-HD, M-HD and CTL plasma. (a) Schematic representation of the workflow followed in both plasma subfractions. (b) Representative profiles of CTL and HD plasma SEC fractions by protein determination and EVs fractions eluted in low protein fractions were detected using EV-markers CD9, CD63 and CD81 by flow cytometry analysis. (c) Fold change of MFI values (MFI values compared to the isotype control—IgG-) for CD9, CD63, and CD81 in EVs pooled fractions ($n = 8$–10 per group). (d) Representative Western Blot analysis of EVs fractions for the presence of EV markers (Flotillin1, TSG101 and Alix) and negative EV-markers (COX IV and Calnexin). SH-SY5Y cell lysate (SH) was used as a positive control ($n = 3$ per group). (e) NTA size distribution profiles of EVs fractions (left) and quantification of EV particle concentration (right) (CTL vs. P-HD, adj $p = 0.984$; CTL vs. M-HD, adj $p = 0.348$; P-HD vs. M-HD, adj $p = 0.432$; $n = 5$ per group). (f) Representative images of cryo-EM of P-HD, M-HD and CTL EVs. Bar = 200 nm ($n = 5$ per group). (g) Size distribution of EVs diameter by cryo-EM ($n = 5$ per group). (h) Protein content of NonEVs fractions ($n = 8$–10 per group). sRNA profiles analyzed by SeqCluster tool showing the fraction of reads that align to small RNA types per plasma group (i) in EVs fractions and (j) NonEVs fractions ($n = 10$ per group). Coefficient of variance (CV) in EV fraction = 0.09; CV in NonEVs fraction = 1.1; Levene's test used to assess the equality of variances, between EVs and NonEVs (p-value = 0.0027). All data are represented as Mean ± SD.

groups at any size range (Figure 2g). In NonEVs fractions, the measurement of total protein concentration in the three groups rendered similar results (Figure 2h).

3.3 | Heterogeneous diversity of extracellular sRNAs in CTL and *HTT* mutation carriers

To uncover the sRNA diversity in the two selected plasma fractions between *HTT* mutation carriers and control samples, we characterized the sRNA profiles in the EVs and NonEVs selected fractions by deep sequencing and applied diverse supervised and unsupervised statistical methods to capture differently expressed sRNAs (Figure 2a). As observed in the proof of concept (Figures 1f and S3a), most reads mapped onto rRNA (51%) followed by gene fragments (34%), and a comparable total number of different sRNA clusters were identified in the three groups (Figure 2i,j and S6a,b). However, we observed heterogeneous proportions of some sRNAs biotypes in the two plasma fractions, including miRNAs and tRFs (Figure 2i,j), in line with the initial plasma subfractionation analysis (Figure 1).

It is worth mentioning that sequencing analyses revealed low levels of miRNAs which accounted for less than 5% of the EVs-sRNA content in the three groups of samples (Figure 2i) as previously shown (Srinivasan et al., 2019). The analysis of the NonEV fractions suggested an increased proportion of miRNAs in mutation carriers (Figure 2j); however, DESeq analyses did not reveal significant deregulation in P-HD mutation carriers and few miRNAs were upregulated at manifest stages (Figure S7a,b, Tables S2 and S3). In line with these observations, we failed to validate the deregulation pattern of selected candidates in additional samples (Figure S7c). This may be related to the significant increase of the inter-sample variability in sRNAs levels in NonEV compared with EV fractions (Figures 2i,j and S6c,d), revealed by the comparison of the coefficient of variation (CV) between the two plasma fractions (CV in EVs fraction = 0.09; CV in NonEVs fraction = 1.1; p-value = 0.0027 based on Levene's test for homogeneity of variances). Another obvious sign of increased heterogeneity in the NonEV fraction within the three groups of patients is detected in the read length profiles obtained in the descriptive analysis of sequencing data (Figure S1b).

In contrast, in the EV fractions, probably due to the conferred vesicular protection, the proportions of sRNAs are more homogeneous between individuals (Figures 2i and S6c). Thus, we opted to proceed with the downstream analyses only in the vesicular compartment.

3.4 | Specific exRNAs-EVs correlate with cognitive and motor performance in HTT mutation carriers

A differential expression analysis focused on the EV fraction highlighted a significant downregulation of most sRNAs in *HTT* mutation carriers compared to CTL samples, with many downregulated sRNAs shared between P-HD and M-HD (Figures 3a–c and S8a–c; Tables S4 and S5).

To highlight specific expression patterns of sRNAs that discriminate between groups, we selected miRNAs and tRFs as reliable types of sRNAs, along with gene fragments as abundant differentially expressed species. We applied highly strict PLS-DA models to show specific expression patterns of sRNAs discriminating groups (see Section 2) (Tables S6 and S7). sRNAs with the highest contributions were then selected for unsupervised principal component analysis (PCA). The first two components of the PCA showed that P-HD and M-HD clearly separated from healthy controls (Figure 3d), while separation was not so obvious between P-HD and M-HD, which could be better achieved when using sRNAs identified with the ExceRpt tool (Figure S8d).

To gain insight into the association of DE sRNAs (miRNAs, tRFs and gene fragments) and the disease, we defined meaningful sets of sRNAs specific for the P-HD group, M-HD group, and P-HD and M-HD group and explored the correlation between their expression levels and patients' clinical features considered during the HD course. To identify significant sets of sRNAs, we used DE sRNAs in P-HD and/or M-HD compared to CTL samples (adj $p < 0.05$) showing considerable importance in the PLS-DA frameworks (see Section 2). Then, we employed linear regression models to evaluate the association of each of these DE-sRNA (adjusted by age and sex) with each component of the cUHDRS, which includes the SWRT, SDMT, UHDRS-TMS, and TFC. This allowed the identification of three smaller sets of sRNAs significantly associated with cUHDRS (p-value < 0.05): 12 DE sRNAs in P-HD, 17 DE sRNAs in P-HD and M-HD, and 48 sRNAs DE in M-HD (Figure 4b and Table S8). To evaluate the multivariate association between these sets of sRNAs with any of the cUHDRS components, we performed an age- and sex-adjusted PLSR analysis (Table 2). Noticeably, we observed that the expression pattern of the P-HD specific set of sRNAs was significantly associated with the SWRT test in *HTT* mutation carriers (P-HD and M-HD) (Figure 4c and Table 2; coefficient of determination (R^2) = 0.97; p-value < 0.0001). Moreover, when we restricted the analysis to the P-HD group, the association of this set of sRNAs and SWRT was still maintained (Figure 4d, Table 2; R^2 = 0.93; p-value = 0.04) while no association was observed when only considering the M-HD group (Figure 4e, Table 2; R^2 = 0.29; p-value = 0.74), suggesting that the joined expression pattern of a specific set of P-HD-sRNAs can highlight pre-clinical changes. To assess to what extent the correlation observed between SWRT score and the set of top DE sRNAs in P-HD is mainly due to the disease and or a consequence of population diversity, we repeated the analysis including the CTL samples, and observed that the association lost significance

TABLE 2 Correlation of EV DE sRNAs and clinical measures in HTT mutation-carriers.

	Groups included	SWRT	SDMT	UHDRS-TMS	TFC	cUHDRS
sRNAs DE in P-HD (12)	P-HD, M-HD (n = 20)	**0.97 (p-value < 0.0001)**	0.16 (p-value: 0.62)	–	–	0.19 (p-value: 0.79)
	P-HD (n = 10)	**0.93 (p-value: 0.04)**	0.38 (p-value: 0.72)	–	–	0.65 (p-value: 0.24)
	M-HD (n = 10)	0.29 (p-value: 0.74)	0.29 (p-value: 0.58)	0.297 (p-value: 0.79)	0.37 (p-value: 0.79)	0.28 (p-value: 0.88)
sRNAs DE in P-HD & M-HD (17)	P-HD, M-HD (n = 20)	0.31 (p-value: 0.51)	0.34 (p-value: 0.25)	–	–	0.41 (p-value: 0.13)
	P-HD (n = 10)	0.62 (p-value: 0.41)	0.59 (p-value: 0.30)	–	–	0.42 (p-value: 0.79)
	M-HD (n = 10)	0.59 (p-value: 0.18)	0.50 (p-value: 0.18)	0.44 (p-value: 0.39)	0.53 (p-value: 0.23)	0.56 (p-value: 0.17)
sRNAs DE in M-HD (49)	P-HD, M-HD (n = 20)	0.24 (p-value: 0.97)	0.15 (p-value: 0.99)	–	–	0.17 (p-value: 1)
	P-HD (n = 10)	0.39 (p-value: 0.99)	0.06 (p-value: 1)	–	–	0.18 (p-value: 1)
	M-HD (n = 10)	**0.85 (p-value: 0.03)**	0.69 (p-value: 0.07)	**0.79 (p-value: 0.004)**	0.46 (p-value: 0.93)	**0.89 (p-value < 0.0001)**

Note: Partial least squares regression sex- and age-adjusted was conducted. Table shows all coefficient of determinations after PLSR age- and sex-adjusted (R2) and p-values. Statiscal significance was defined as $p < 0.05$, with significant values highlighted in bold.

Abbreviations: cUHDRS, Composite Unified Huntington Disease Rating Scale; SWRT, Stroop Word Reading Test; SDMT, Symbol Digit Modality Test; TFC, total functional capacity; UHDRS-TMS, Unified Huntington Disease Rating Scale–Total Motor Score.

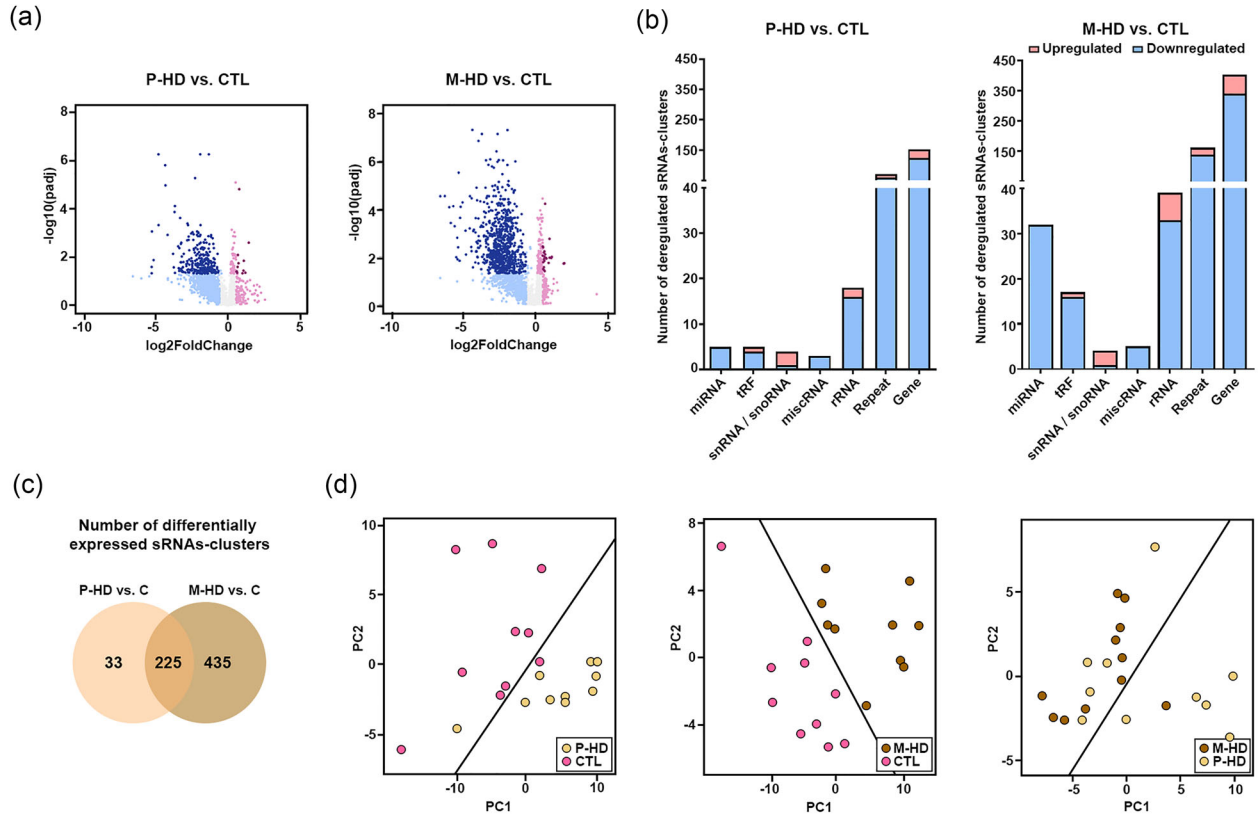

FIGURE 3 sRNAs from HD patients are deregulated in EVs fractions in comparison to CTL samples, using SeqCluster tool. (a) Volcano plots showing DE sRNAs-clusters in P-HD-EVs versus CTL-EVs fractions and M-HD-EVs versus CTL-EVs fractions. Dark pink dots and dark blue dots represent significantly upregulated and downregulated genes, respectively (|log2FoldChange| > 0.58, adj $p < 0.05$, $n = 10$ per group). (b) Total number of sRNAs-clusters DE between P-HD-EVs versus CTL-EVs fractions and M-HD-EVs versus CTL-EVs fractions. (c) Venn diagram of DE sRNAs-clusters between P-HD versus CTL and M-HD versus CTL, showing the number of overlapped dysregulated sRNAs-clusters between both comparisons. (d) PCA plots constructed with top DE sRNAs and top sRNA that contribute to discriminating between disease conditions and healthy individuals based on PLS-DA models. The solid line is the linear discriminant function that separates disease conditions.

($R^2 = 0.09$; p-value = 0.82). The expression levels of this specific set of P-HD DE sRNAs did not show a significant correlation with UHDRS-TMS or TFC in M-HD patients, stressing the specific relevance of these species to highlight premanifest cognitive changes (Table 2).

Parallel regression analyses with the set of sRNAs specifically DE in M-HD patients showed significant correlations with SWRT, SDMT, UHDRS-TMS and cUHDRS parameters ($R^2 = 0.85$, p-value = 0.03; $R^2 = 0.69$, p-value = 0.07; $R^2 = 0.79$, p-value = 0.004; and $R^2 = 89$, p-value < 0.0001, respectively) when considering only the manifest group (Table 2). Of notice, the association was lost when the P-HD and CTL groups (UHDRS-TMS score > 5) were included in the analysis. Overall, these data suggest that the combined levels of specific sets of sRNAs can highlight pre-clinical changes and/or symptoms.

3.5 | Sensitivity and specificity of candidate biomarkers for premanifest HD

Although the combined levels of specific sRNAs can finely distinguish P-HD and M-HD clinical changes, the validation of candidate species in independent samples by qPCR, the gold standard technique to quantify sRNAs, is limited by the expression levels of the candidate species and the type of sRNA detected. The expression pattern of specific gene fragments selected from the refined lists of meaningful sRNAs (Table S8) was not validated (Figure S9), differing from miR-451a and tRF-Lys-TTT, selected from the same lists (Figure 5a). While the latter are well-established sRNAs defined by a dominating sequence, clusters of gene fragments are represented by the sum of multiple abundant sequences derived from a gene (see Section 2). Thus, a custom qPCR directed to a specific sequence may readily validate the expression pattern of a real sRNA and may not easily capture the expression pattern and complexity of the gene-derived fragments.

Thus, to explore potential new biomarkers in HD and validate the sRNA-sequencing results, our focus was on recognized sRNAs, including miRNAs and tRFs, consistently detected through sequencing approaches. We selected eight candidate sRNAs (DE sRNAs showing a p-adj < 0.05 in P-HD vs. CTL and/or in M-HD vs. CTL, with a base mean sequence reads > 200, and

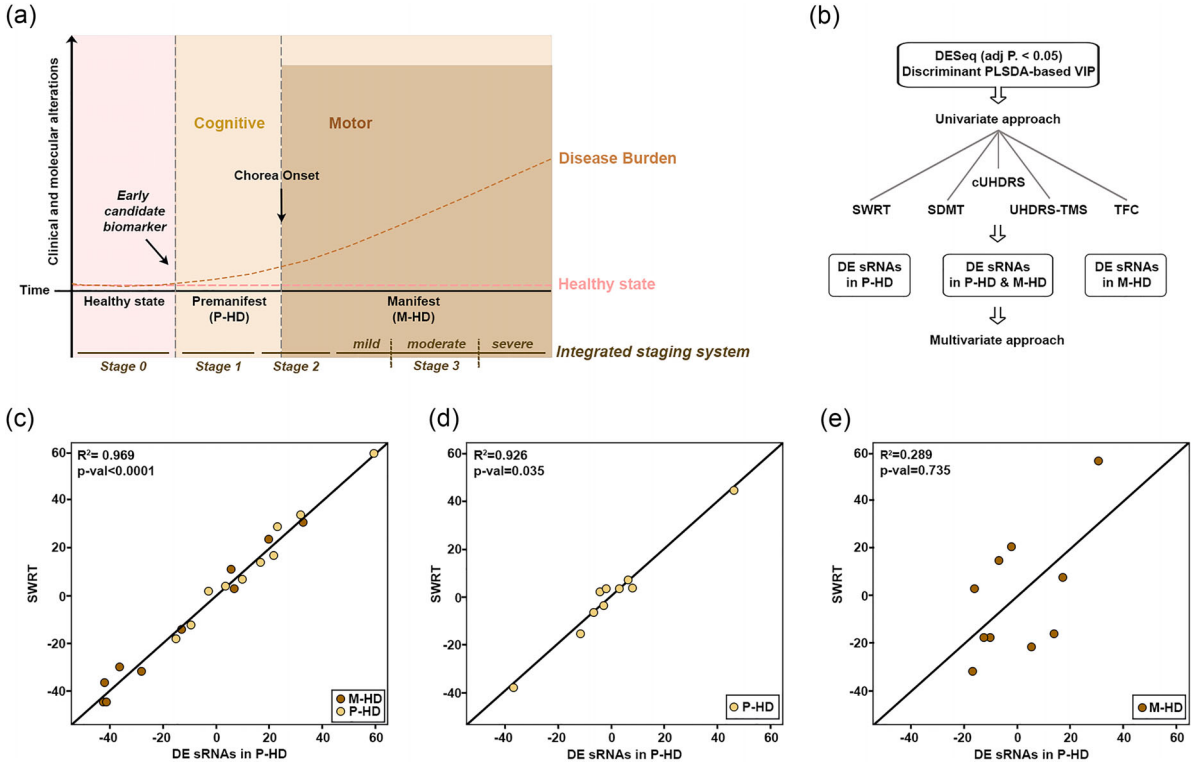

FIGURE 4 sRNAs deregulated in premanifest stages correlate with cognitive symptomatology. (a) The framework of Huntington's Disease stages. The ideal candidate molecular biomarker would be measurable prior to the appearance of P-HD and M-HD symptoms and would correlate with the disease course. The current patients' classification system together with the Integrated staging system[74] is depicted. (b) Workflow followed to select relevant sRNAs for correlation analyses. PLSR analysis depicting the relation between the set of sRNAs specifically DE in P-HD patients and the performance of the SWRT test (c) in HTT mutation carriers (P-HD and M-HD; $R^2 = 0.97$; p-value < 0.0001); (d) only in the P-HD group ($R^2 = 0.93$; p-value = 0.035); and (e) only in the M-HD group ($R^2 = 0.289$; p-value = 0.735).

high contribution to PLSDA discrimination) for qRT-PCR determinations. We validated their relative expression in the set of samples used for sRNA-sequencing (Table 1) and in an added independent biological set of samples (Table 3) obtaining a total size of validation of 20–21 samples per group (Table S1). Due to the absence of universal endogenous sRNA normalizers, hsa-miR-100-5p was selected as the reference gene since it was a highly stable sRNA with low variability among all the sequenced samples (Figure S10).

According to qRT-PCR results, miR-451a, miR-21-5p, miR-26a-5p, let-7a-5p, miR-27a-3p, tRF-Glu-CTC and tRF-Gly-GCC expression was significantly downregulated in P-HD and M-HD in comparison to CTL samples, consistent with the sequencing findings. Moreover, tRF-Lys-TTT expression showed an analogous downregulation between M-HD versus CTL samples, considering an unadjusted p-value of 0.015 (Figure 5a).

To evaluate the sensitivity of the qRT-PCR validated sRNAs as biomarkers for early HD stages, we analyzed their biomarker prediction outcome. At the same time, we compared it with the diagnostic potential of NfL in the same group, as it is considered the most sensitive blood biomarker in HD (Figure 5b). sRNAs individually showed a similar diagnostic potential compared to NfL (Figures 5c and S11a). Of note, our data indicate that the combination of 2, 3 or 4 validated sRNAs showed similar specificity and sensitivity discriminating between P-HD patients and healthy individuals (Figures 5d,e and S11b). For instance, the performance of an ensemble of 2-sRNAs-biosignature including tRF-Gly-GCC and miR-27a-3p presented an AUC = 0.863 (CI = 0.74-0.99, Figure 5d), and the ensemble of 3-sRNAs-biosignature being tRF-Glu-CTC, tRF-Gly-GCC and miR-27a-3p, reached an AUC = 0.88 (CI = 0.76–0.99, Figure 5e).

Moreover, using these sets of patients and considering plasma NfL levels in combination with our validated sRNAs, we also estimated a high diagnosis potential. Specifically, the combined biosignature of tRF-Gly-GCC and miR-27a-3p, together with plasma NfL showed an AUC = 0.908 (CI = 0.82–0.99) (Figure S11c).

3.6 | miR-21-5p as a progression biomarker at premanifest HD stage

Finally, to explore the potential of these sRNAs as progression biomarkers, we analyzed their expression in nine P-HD patients for whom we had paired plasma samples from a 1.5-year follow-up visit (Table S1). Specifically, miR-21-5p expression was

TABLE 3 Clinic and sociodemographic characteristics of added independent samples used for qPCR validation.

	Total	CTL	P-HD	M-HD
Age (years)	47.2 ± 12.55	37.93 ± 15.67	38.88 ± 4.97	50.70 ± 9.85
Sex (m/f)	11/19	6/4	5/6	6/4
CAG	–	–	42.5 ± 1.51	42.30 ± 1.95
DBS[a]	–	–	274.42 ± 83.01	342.21 ± 55.52
cUHDRS[b]	–	17.87 ± 1.30	17.27 ± 1.74	11.41 ± 4.91
UHDRS-TMS[c]	–	0	2.00 ± 2.05	23.38 ± 17.03
TFC[d]	–	13 ± 0	12.90 ± 0.32	10.75 ± 2.96
SWRT[e]	–	111.25 ± 15.78	97.1 ± 17.27	74.63 ± 26.33
SDMT[f]	–	54.00 ± 7.62	57.30 ± 11.23	32.63 ± 15.96
Plasma NfL (pg/mL)	–	4.41 ± 2.01	14.69 ± 8.17	24.88 ± 10.12

[a]Disease Burden Score as measured by age × (CAG-35.5).
[b]Composite Unified Huntington Disease Rating Scale.
[c]Unified Huntington Disease Rating Scale–Total Motor Score.
[d]Total Functional Capacity.
[e]Stroop Word Reading Test.
[f]Symbol Digit Modality Test.

significantly decreased over time, indicating that it could act as progression biomarker at premanifest stages of the disease (Figure 6).

We further evaluated the correlation between individual sRNAs and the patients' clinical features (Table 4). We observed that the expression of miR-21-5p and miR-26a-5p significantly correlated with SDMT and cUHDRS when only P-HD individuals were considered, supporting these miRNAs as biomarkers sensing preclinical changes. Furthermore, these results suggest that miR-21-5p could be a progression biomarker to monitor longitudinal clinical changes occurring during the premanifest stage. Parallel correlation analyses with NfL and the clinical measures were performed, but significant association was only found when considering the ensemble of P-HD and M-HD groups (Table 4), as previously reported (Byrne et al., 2017; Parkin et al., 2021).

4 | DISCUSSION

In HD, the identification of early molecular alterations in premanifest individuals, occurring before the motor-based clinical diagnosis is of outmost importance, as it provides an opportunity to monitor disease progression and achieve clinical management of the patients in an individual manner. Biofluid sRNAs are a promising source of early biomarkers since their expression levels are highly sensitive to physiological and pathological changes. In HD this is reinforced by the fact that sRNAs are profoundly altered in the brain and these perturbations have been directly linked to HD pathogenesis (Creus-Muncunill et al., 2021; Langfelder et al., 2018; Martí et al., 2010). Thus, in addition to clinical measures, sRNA profiling offers opportunities for the direct quantification of pathobiological processes at the molecular level. In the present study, we have deeply analyzed sRNA profiles in plasma subfractions and uncovered specific EVs-sRNAs as potential markers to monitor premanifest changes.

A major challenge in reliable and reproducible sRNA biomarker discovery is the identification of an informative biofluid compartment. Here we have identified differentiated sRNA profiles in EVs (cEVs) and extravesicular, protein enriched (NonEVs-High) plasma subfractions, confirming the idea that diverse plasma carriers offer scenarios for differential distribution of exRNAs (Murillo et al., 2019). Although not all SEC-fractions were analyzed, it became apparent that cEVs were a suitable source to analyze sRNAs as biomarkers, showing greater homogeneity compared with NonEVs-High fraction. As widely discussed elsewhere (Heitzer et al., 2019; Moufarrej et al., 2022), EV-sRNAs are highly resistant to degradation, which may contribute to more consistent and uniform exRNA profiles.

In HD, several studies have been focused on the exploration of brain and CSF miRNAs expression (Ghafouri-Fard et al., 2022; Hoss et al., 2015; Reed et al., 2018). However, little information is available regarding dynamic changes of sRNAs in plasma, and none has studied plasma-EVs as a source of biomarkers. Furthermore, while exRNA biomarker research is mainly focused on miRNAs we showed that miRNAs represent a minor proportion of the EVs transcriptome, in line with previous reports (Albanese et al., 2021; Jeppesen et al., 2019; Lässer et al., 2017; Schageman et al., 2013; Srinivasan et al., 2019), and other species including tRFs and YRNAs are highly represented.

Here, we have shown that most of the plasma EVs-derived sRNAs are downregulated in mutation carriers compared with CTL, with more significant changes at manifest stages. Previously reported upregulated miRNAs in plasma of HD patients (Díez-Planelles et al., 2016; Hoss et al., 2015) including miR-10b-5p, miR-486-5p, miR-30d-5p and miR-222-3p were not validated in the present study. In addition, the observed downregulated miR-27a-3p and miR-21-5p were significantly overexpressed in analyses

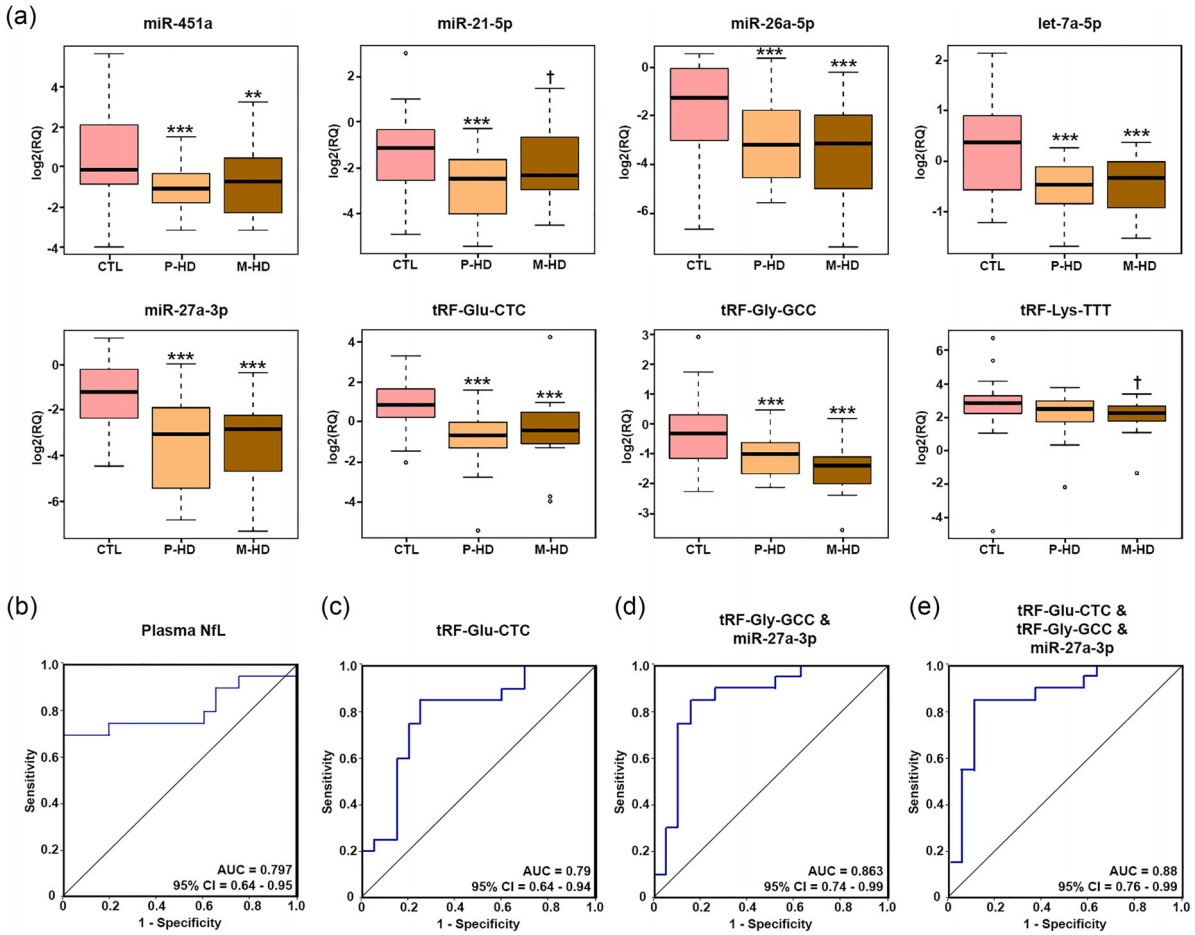

FIGURE 5 Validation and diagnostic potential analysis of selected sRNAs at premanifest stages. (a) Boxplots representing the relative expression of sRNAs validated with qRT-PCR in the group of samples used for sRNA sequencing ($n = 10$ per group) and in an added independent biological group of samples ($n = 10$–11 per group). Significant differences between P-HD and M-HD vs- CTL groups are presented with *** (adj $p < 0.001$), ** (adj $p < 0.01$) and nominally significant differences are presented with † (p-value < 0.05). (b) ROC curves analysis of the sensitivity and specificity of plasma NfL between P-HD and CTL (p-value = 0.001). (c) Representative ROC curve analysis of the sensitivity and specificity of an individual validated sRNA: tRF-Glu-CTC between P-HD and CTL (p-value = 0.002). (d) ROC curves analysis of the sensitivity and specificity of a novel 2-sRNAs-biosignature: an ensemble of tRF-Gly-GCC and miR-27a-3p between P-HD and CTL (p-value = 0.0001). (e) ROC curves analysis of the sensitivity and specificity of a novel 3-sRNAs-biosignature: the ensemble of tRF-Glu-CTC, tRF-Gly-GCC and miR-27a-3p between P-HD and CTL (p-value = 0.0001). $n = 20$-21 per group.

of total plasma as reported by Díez-Planelles et al. (2016). Overall, these data suggest that the specific EVs miRNA content may offer complementary information regarding HD status.

The massive downregulation of sRNAs observed at premanifest and manifest stages in HD-EVs might reflect an altered vesicular sRNA-packaging mechanism. Currently, the specific pathways involved in the RNA packaging in EVs remain unknown (Margolis & Sadovsky, 2019). However, studies are increasingly revealing that active sorting and loading of coding and non-coding RNAs in EVs may be controlled by RNA-binding proteins. These include the hnRNP family (Fabbiano et al., 2020; Luo et al., 2021) and/or via ESCRT dependent or independent pathways (Corrado et al., 2021), including Alix adaptor protein involved in EVs biogenesis and cargo sorting through an ESCRT dependent pathway (Larios et al., 2020). Recent evidence indicates that Alix forms a complex with the RNA binding protein Ago2 involved in miRNA transport and processing and drives associated miRNAs into EVs. Ago2 has been recently shown to be strongly downregulated in HD human brains (Petry et al., 2022). Whether Ago2 decrease is extensive to other tissues/organs that contribute to circulating EVs remains to be elucidated; however, it is tempting to speculate that decreased Ago 2 in HD underlies the general impaired miRNA loading into EVs. Furthermore, whether alterations of additional RNA-binding proteins could lead to perturbations in the RNA content of HD EVs remains to be answered.

Among the validated HD-EVs decreased miRNAs, miR-451a and let-7a are up- and downregulated respectively in HD brains (Martí et al., 2010). MiR-451a participates in neuroinflammation, oxidative stress and neuronal apoptosis associated with ischemic cerebral damage (Fu et al., 2019; Wang et al., 2021); and let-7a-5p regulates inflammation in other neurodegenerative conditions (Wang, 2023). Interestingly, these miRNAs have been detected in neuronal-enriched EVs obtained from total plasma (Durur et al.,

TABLE 4 Correlation of EV-sRNAs biosignature as measured by qRT-PCR and plasma NfL levels with clinical measures in HTT mutation-carriers.

	Groups included	SWRT	SDMT	UHDRS-TMS	TFC	cUHDRS
miR-451a	P-HD, M-HD ($n = 40$)	−0.006 (p-value: 0.97)	−0.06 (p-value: 0.71)	–	–	−0.10 (p-value: 0.53)
	P-HD ($n = 20$)	0.16 (p-value: 0.51)	−0.39 (p-value: 0.09)	–	–	−0.28 (p-value: 0.24)
	M-HD ($n = 20$)	0.08 (p-value:0.74)	0.36 (p-value: 0.16)	−0.09 (0.73)	0.05 (p-value: 0.85)	0.19 (p-value: 0.45)
miR-21-5p	P-HD, M-HD ($n = 40$)	−0.03 (p-value: 0.87)	−0.16 (p-value: 0.35)	–	–	−0.22 (p-value: 0.19)
	P-HD ($n = 20$)	−0.22 (p-value: 0.37)	**−0.57 (p-value: 0.01)**	–	–	**−0.65 (p-value: 0.003)**
	M-HD ($n = 20$)	0.35 (p-value: 0.18)	0.34 (p-value: 0.19)	−0.11 (p-value: 0.68)	−0.06 (p-value: 0.82)	0.26 (p-value: 0.34)
let-7a-5p	P-HD, M-HD ($n = 40$)	−0.14 (p-value: 0.4)	0.03 (p-value:0.86)	–	–	−0.04 (p-value: 0.79)
	P-HD ($n = 20$)	−0.06 (p-value: 0.79)	0.20 (p-value: 0.41)	–	–	−0.07 (p-value: 0.77)
	M-HD ($n = 20$)	−0.11 (p-value: 0.68)	0.08 (p-value: 0.77)	−0.11 (p-value: 0.66)	0.04 (p-value: 0.86)	0.14 (p-value: 0.60)
miR-27a-3p	P-HD, M-HD ($n = 40$)	0.23 (p-value: 0.16)	0.07 (p-value: 0.68)	–	–	0.10 (p-value:0.54)
	P-HD ($n = 20$)	−0.06 (p-value: 0.82)	−0.46 (p-value: 0.05)	–	–	−0.40 (p-value: 0.08)
	M-HD ($n = 20$)	**0.54 (p-value: 0.02)**	0.46 (p-value: 0.06)	−0.48 (p-value: 0.05)	0.29 (p-value: 0.24)	**0.53 (p-value: 0.03)**
miR-26a-5p	P-HD, M-HD ($n = 40$)	0.16 (p-value: 0.33)	0.11 (p-value: 0.53)	–	–	0.12 (p-value: 0.49)
	P-HD ($n = 20$)	−0.12 (p-value: 0.63)	**−0.61 (p-value: 0.006)**	–	–	**−0.56 (p-value: 0.01)**
	M-HD ($n = 20$)	0.38 (p-value: 0.13)	0.44 (p-value: 0.08)	**−0.5 (p-value: 0.03)**	0.33 (p-value: 0.20)	0.46 (p-value: 0.06)
tRNA-Glu-CTC	P-HD, M-HD ($n = 40$)	0.02 (p-value: 0.92)	−0.07 (p-value: 0.66)	–	–	−0.07 (p-value: 0.69)
	P-HD ($n = 20$)	0.14 (p-value: 0.58)	0.013 (p-value: 0.96)	–	–	−0.05 (p-value: 0.84)
	M-HD ($n = 20$)	0.10 (p-value: 0.69)	0.08 (p-value: 0.76)	−0.25 (p-value: 0.33)	0.11 (p-value:0.66)	0.17 (p-value: 0.5)
tRNA-Gly-GCC	P-HD, M-HD ($n = 40$)	0.05 (p-value: 0.79)	0.13 (p-value: 0.45)	–	–	0.14 (p-value: 0.41)
	P-HD ($n = 20$)	0.09 (p-value: 0.71)	0.01 (p-value: 0.96)	–	–	0.03 (p-value: 0.89)
	M-HD ($n = 20$)	0.10 (p-value: 0.69)	0.14 (p-value: 0.59)	−0.31 (p-value: 0.22)	0.12 (p-value: 0.64)	0.23 (p-value: 0.38)
tRNA-Lys-TTT	P-HD, M-HD ($n = 40$)	0.07 (p-value: 0.67)	−0.12 (p-value: 049)	–	–	−0.03 (p-value: 0.83)
	P-HD ($n = 20$)	0.32 (p-value: 0.18)	−0.44 (p-value: 0.06)	–	–	−0.19 (p-value: 0.42)
	M-HD ($n = 20$)	−0.14 (p-value: 0.59)	0.05 (p-value: 0.83)	−0.04 (p-value: 088)	0.01 (p-value: 0.97)	−0.03 (p-value: 0.90)
Plasma NfL	P-HD, M-HD ($n = 40$)	**−0.45 (p-value: 0.01)**	**−0.43 (p-value: 0.01)**	–	–	**−0.56 (p-value < 0.001)**
	P-HD ($n = 20$)	−0.11(p-value: 0.67)	−0.007 (p-value: 0.98)	–	–	−0.09 (p-value: 0.70)
	M-HD ($n = 20$)	−0.30 (p-value: 0.27)	−0.24 (p-value: 0.39)	0.47 (p-value: 0.08)	−0.41 (p-value: 0.13)	−0.41 (p-value: 0.13)

Note: All analyses were conducted using Spearman's correlation and nonparametric partial correlation tests for sex and age-adjusting. Table shows the spearman rank correlation coefficient (rho) and p-values. Statistical significance was defined as p-value < 0.05, with significant values highlighted in bold.

Abbreviations: cUHDRS, Composite Unified Huntington Disease Rating Scale; SWRT, Stroop Word Reading Test; SDMT, Symbol Digit Modality Test; TFC, total functional capacity; UHDRS_TMS, Unified Huntington Disease Rating Scale-Total Motor Score.

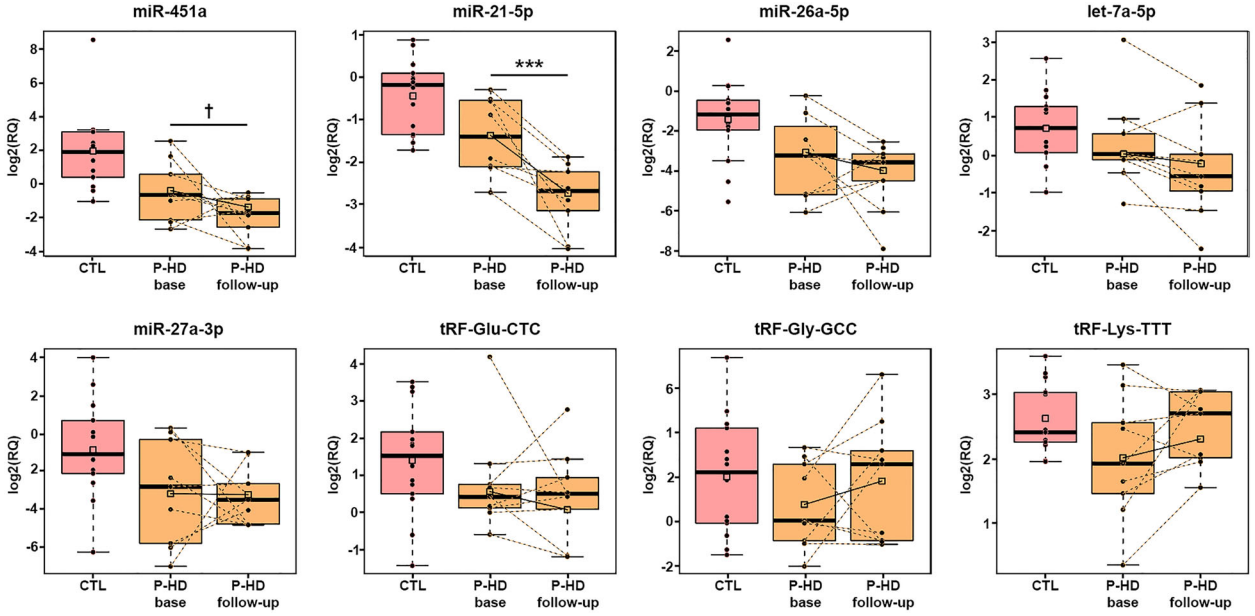

FIGURE 6 Longitudinal changes validation of selected sRNAs at premanifest stages over a 1.5-year follow-up. Boxplots representing the relative expression of sRNAs validated by qRT-PCR in P-HD paired samples from baseline and 1.5-year follow-up visits. Squares represent mean values. Significant differences between longitudinal samples are presented with *** (adj $p < 0.001$), ** (adj $p < 0.01$), * (adj $p < 0.05$) and nominally significant differences are presented with † (p-value < 0.05). $n = 9$ samples per group.

2022), suggesting that the DE observed in plasma HD-EVs partially reflects changes occurring in the brain. In the discovery phase of the present analysis, sequencing data suggest additional DE miRNAs with some reported to be altered in HD brains (Table S9). Whether brain DE sRNAs contribute to HD neuropathology and if their altered cargo in plasma EVs reflects progressive dysfunction is a complex question, that needs integration of molecular, functional and systemic data.

Our study shows that beyond miRNAs, tRF-Gly-GCC and tRF-Glu-CTC are early altered in mutation carriers. These species have been recently revealed as highly abundant and stable in circulation (Costa et al., 2023; Yeri et al., 2017), pointing them as promising pre-manifest biomarkers in HD. In addition, in HD, strong deregulation of these species, including the EV-validated tRF-Gly-GCC and tRF-Glu-CTC, has been detected in the putamen of patients (Creus-Muncunill et al., 2021), and functional analysis suggests a role of diverse tRFs in neuronal dysfunction (Creus-Muncunill et al., 2021). Future studies should determine whether the dynamic expression of circulating tRFs reflects brain alterations.

HD clinical alterations emerge gradually during a premanifest phase, and the precise shift from premanifest to manifest HD may be difficult to anticipate (Figure 4a). Subtle cognitive changes can be detected in premanifest population up to 15 years before diagnosis in specific measures addressing processing speed and attention (Paulsen et al., 2017). This is the case of the SWRT whose linear worsening has been extensively reported to occur from the premanifest stage of the disease. Based on sequencing data analysis, we have observed that the expression of a specific set of DE sRNAs in P-HD (and not in M-HD) was strongly associated with SWRT score using the P-HD group (either individually or with M-HD), but this specific sRNA-P-HD set did not associate with UHDRS-TMS when using the M-HD group of patients. Complementing this finding, a set of sRNAs specifically DE in M-HD significantly correlated with UHDRS-TMS and cognitive performance (SWRT and SDMT) when evaluating the M-HD group, but not when using the P-HD samples, either alone or together with M-HD. These data indicate that specific sets of sRNAs may distinguish premanifest alterations and manifest symptomatology, pointing them as highly sensitive biomarkers.

The translational utility of these findings is limited by the sensitivity of the current techniques (qRT-PCR) to detect low-abundant sRNAs and the type of candidate sRNAs. Several sRNAs within the specific sets that significantly correlate with clinical signs correspond to gene fragments. Many of the altered gene fragments (sRNAs annotating onto genes) may provide an indirect measure of the levels of changing genes rather than bona fide sRNAs that can be proposed as reliable molecular biomarkers. Therefore, subsequent follow-up validation in additional samples focused on genuine sRNAs such as miRNAs and tRFs consistently detected and significantly DE according to sequencing data analysis. The successful validation of 7 out of 8 distinct sRNAs candidates by qRT-PCR in independent samples confirmed the robustness of our sRNA-seq analysis pipeline. Interestingly, the follow-up validation experiment in a group of P-HD patients revealed the potential of miR-21-5p as pre-clinical progression biomarker. Of notice, when using P-HD samples individually, miR-21-5p and miR-26a-5p were significantly correlated with SDMT, which gradually indexes disease progression at these pre-motor stages (Carlozzi et al., 2014), and with cUHDRS. On the other hand, we failed to obtain a significant correlation between NfL plasma levels and clinical data in this set of premanifest samples, which was only reached when using P-HD and M-HD groups together, validating what has recently been published

(Byrne et al., 2017; Parkin et al., 2021). NfL is rising as a reference biomarker reflecting neuronal injury in multiple neurodegenerative disorders. However, the present results suggest that NfL presents a limited utility as a tracking measure for premanifest changes, which could be overcome by analyzing it in combination with specific sRNAs.

Confirming previous studies (Parkin et al., 2021), our results indicate that NfL levels could strongly distinguish M-HD from both P-HD and Control groups. Candidate sRNAs and NfL displayed a similar discriminative performance between P-HD or M-HD and CTLs; however, sRNAs could not differentiate between P-HD and M-HD groups. Overall, these data indicate a clear progression of neuronal damage and axonal injury from premanifest to manifest stages (NfL levels) that was not mirrored by the selected candidate sRNAs, strongly altered at both stages. Nevertheless, the robust alteration of specific sRNAs at premanifest stages suggests that these species may finely indicate early perturbations occurring long before obvious neurodegeneration. Supporting this hypothesis, changes in gene expression at the transcriptional level (both mRNA and miRNA) occur in the brain of HD mouse models before the onset of motor and cognitive alterations, and striatal cell loss (Langfelder et al., 2016, 2018).

Thus, studying sRNAs that reflect changes occurring before the onset of neurodegeneration and clinical symptoms, appears to be a promising approach to better classify mutation carriers at premanifest stages of HD. Specifically, this approach could aid in the stratification of individuals in Stage 0 to Stage 1 of the Integrated Staging System for the classification of HD (as shown in Figure 4a), which was developed to address the need for better subclassification criteria in the pre-motor HD stages (Tabrizi et al., 2022).

Despite these findings, there are still several limitations in our study. Notably, the clinical implementation of RNA-based biomarkers in EVs demands rigorous analytical validation and standardized procedures for EV isolation, RNA extraction, and detection of specific species. These requirements are mandatory to ensure the reliability and applicability of EV-based biomarkers in clinical settings. In addition, we acknowledge the risk of over-fitting RNAseq for biomarker discovery. While we have conducted in-depth analysis of sRNA profiles in a discovery cohort and validated specific candidates in a larger group of patients, further confirmatory studies in multi-centre settings with larger cohorts and extended follow-up periods from different geographic locations are necessary. Moreover, the relatively short follow-up time does not allow interpretation of our findings in relation to significant aggravation of clinical symptomatology.

In summary, our results demonstrate that, among the heterogenous sRNA plasma composition, encapsulated EV-sRNAs are early deregulated in HD, and that this deregulation might be associated with early changes occurring at pre-motor phases of the disease. Altogether, these findings present a compelling argument to consider specific sRNAs, including diverse biotypes such as tRFs, as promising HD biomarkers.

AUTHOR CONTRIBUTIONS

Marina Herrero-Lorenzo: Conceptualization (equal); data curation (equal); formal analysis (equal); investigation (equal); methodology (equal); resources (equal); validation (equal); visualization (equal); writing—original draft (equal); writing—review and editing (equal). **Jesús Pérez-Pérez**: Data curation (supporting); investigation (equal); writing—review and editing (supporting). **Georgia Escaramís**: Conceptualization (equal); data curation (equal); formal analysis (equal); software (equal); supervision (equal); validation (equal); writing—original draft (equal); writing—review and editing (equal). **Saül Martínez-Horta**: Data curation(supporting); Investigation(equal); Writing—review & editing(supporting). **Rocío Pérez-González**: Data curation (supporting); resources (equal); writing—review and editing (supporting). **Elisa Rivas-Asensio**: Investigation (equal); writing—review and editing (supporting). **Jaime Kulisevsky**: Writing—review and editing (supporting). **Ana Gámez-Valero**: Conceptualization (equal); formal analysis (supporting); funding acquisition (equal); investigation (equal); methodology (equal); project administration (equal); supervision (equal); writing—original draft (equal); writing—review and editing (equal). **Eulàlia Martí**: Conceptualization(equal); Funding acquisition(lead); Investigation(equal); Project administration(equal); Supervision(equal); Writing—original draft(equal); Writing—review & editing(equal).

ACKNOWLEDGEMENTS

The authors would like to thank all patients at the Hospital de la Santa Creu I Sant Pau and volunteers involved in the study for providing plasma samples. In particular, we want to thank the nurses Claudia Palomera and Andrea García for their involvement in sample collection and processing. The authors would also like to thank Dr. Maria Yañez-Mo (Unidad de Investigación, Hospital Sta Cristina; Departamento Biología Molecular/CBM-SO, UAM) for kindly gifting us antibodies anti-CD9 and anti-CD63 for flow cytometry assays. We wish to thank José Amable Bernabé for his fast measurements of EVs by NTA. It has been performed by the ICTS 'NANBIOSIS', Unit 6, unit of the CIBER in Bioengineering, Biomaterials & Nanomedicne (CIBER-BBN) at the Barcelona Materials Science Institute. Also, we thank Martí de Cabo for acquiring excellent images of EVs by cryo-EM (Servei de Microscòpia, Universitat Autónoma de Barcelona). We thank the staff of Genomics Unit at the CRG for the preparation of sRNA libraries and sRNA sequencing. We wish to gratefully acknowledge Luisa Mariscal and Sonia Jansa from bioNova for generously providing advice and support regarding sRNA isolation and validation. Finally, we wish to thank Dr. M. Montguió for helpful comments and careful review of the manuscript. This work was supported by the Spanish government through the grant PID2020-113953RB-I00 funded by the Spanish Ministry of Science and Innovation/Spanish State Research Agency (10.13039/501100011033). The study was also supported by a 2021 Human Biology Project from the Huntington's Disease Society of America (HDSA) granted to Ana Gámez-Valero. Ana Gámez-Valero postdoctoral contract was also supported by the 2019

Juan de la Cierva fellowship FJC2019-039633-I. The PhD contract of Marina Herrero-Lorenzo was supported by a fellowship from the Spanish Ministry of Science and Innovation.

CONFLICT OF INTEREST STATEMENT

The authors have declared that no conflict of interest exists.

ORCID

Marina Herrero-Lorenzo https://orcid.org/0000-0003-2693-0700
Jesús Pérez-Pérez https://orcid.org/0000-0002-9835-0484
Georgia Escaramís https://orcid.org/0000-0002-5416-3177
Saül Martínez-Horta https://orcid.org/0000-0003-0125-7249
Rocío Pérez-González https://orcid.org/0000-0002-0641-2001
Jaime Kulisevsky https://orcid.org/0000-0003-4870-1431
Ana Gámez-Valero https://orcid.org/0000-0002-9530-2751
Eulàlia Martí https://orcid.org/0000-0002-1030-3158

REFERENCES

Albanese, M., Chen, Y. A., Hüls, C., Gärtner, K., Tagawa, T., Mejias-Perez, E., Keppler, O. T., Göbel, C., Zeidler, R., Shein, M., Schütz, A. K., & Hammerschmidt, W. (2021). MicroRNAs are minor constituents of extracellular vesicles that are rarely delivered to target cells. *PLoS Genetics*, *17*, e1009951.

Arroyo, J. D., Chevillet, J. R., Kroh, E. M., Ruf, I. K., Pritchard, C. C., Gibson, D. F., Mitchell, P. S., Bennett, C. F., Pogosova-Agadjanyan, E. L., Stirewalt, D. L., Tait, J. F., & Tewari, M. (2011). Argonaute2 complexes carry a population of circulating microRNAs independent of vesicles in human plasma. *Proceedings of the National Academy of Sciences*, *108*, 5003–5008.

Bates, G. P., Dorsey, R., Gusella, J. F., Hayden, M. R., Kay, C., Leavitt, B. R., Nance, M., Ross, C. A., Scahill, R. I., Wetzel, R., Wild, E. J., & Tabrizi, S. J. (2015). Huntington disease. *Nature Reviews Disease Primers*, *1*, 1–21.

Braisch, U., Muche, R., Rothenbacher, D., Landwehrmeyer, G. B., Long, J. D., & Orth, M. (2019). Identification of symbol digit modality test score extremes in Huntington's disease. *American Journal of Medical Genetics, Part B: Neuropsychiatric Genetics*, *180*, 232–245.

Byrne, L. M., Rodrigues, F. B., Blennow, K., Durr, A., Leavitt, B. R., Roos, R. A. C., Scahill, R. I., Tabrizi, S. J., Zetterberg, H., Langbehn, D., & Wild, E. J. (2017). Neurofilament light protein in blood as a potential biomarker of neurodegeneration in Huntington's disease: A retrospective cohort analysis. *Lancet Neurology*, *16*, 601–609.

Carlozzi, N. E., Miciura, A., Migliore, N., & Dayalu, P. (2014). Understanding the outcomes measures used in Huntington disease pharmacological trials: A systematic review. *The Journal of Huntington's Disease*, *3*, 233–252.

Corrado, C., Barreca, M. M., Zichittella, C., Alessandro, R., & Conigliaro, A. (2021). Molecular mediators of RNA loading into extracellular vesicles. *Cells*, *10*, 3355.

Costa, B., Li Calzi, M., Castellano, M., Blanco, V., Cuevasanta, E., Litvan, I., Ivanov, P., Witwer, K., Cayota, A., & Tosar, J. P. (2023). Nicked tRNAs are stable reservoirs of tRNA halves in cells and biofluids. *Proceedings of the National Academy of Sciences*, *120*, e2216330120.

Creus-Muncunill, J., Guisado-Corcoll, A., Venturi, V., Pantano, L., Escaramís, G., García De Herreros, M., Solaguren-Beascoa, M., Gámez-Valero, A., Navarrete, C., Masana, M., Llorens, F., Diaz-Lucena, D., Pérez-Navarro, E., & Martí, E. (2021). Huntington's disease brain-derived small RNAs recapitulate associated neuropathology in mice. *Acta Neuropathologica*, *141*, 565–584.

Díez-Planelles, C., Sánchez-Lozano, P., Crespo, M. C., Gil-Zamorano, J., Ribacoba, R., González, N., Suárez, E., Martínez-Descals, A., Martínez-Camblor, P., Álvarez, V., Martín-Hernández, R., Huerta-Ruíz, I., González-García, I., Cosgaya, J. M., Visioli, F., Dávalos, A., Iglesias-Gutiérrez, E., & Tomás-Zapico, C. (2016). Circulating microRNAs in Huntington's disease: Emerging mediators in metabolic impairment. *Pharmacological Research*, *108*, 102–110.

Dobin, A., Davis, C. A., Schlesinger, F., Drenkow, J., Zaleski, C., Jha, S., Batut, P., Chaisson, M., & Gingeras, T. R. (2013). STAR: Ultrafast universal RNA-seq aligner. *Bioinformatics*, *29*, 15–21.

Dong, X., & Cong, S. (2021). MicroRNAs in Huntington's disease: Diagnostic biomarkers or therapeutic agents? *Frontiers in Cellular Neuroscience*, *15*, 1–10.

Durur, D. Y., Tastan, B., Ugur Tufekci, K., Olcum, M., Uzuner, H., Karakülah, G., Yener, G., & Genc, S. (2022). Alteration of miRNAs in small neuron-derived extracellular vesicles of Alzheimer's disease patients and the effect of extracellular vesicles on microglial immune responses. *Journal of Molecular Neuroscience*, *72*, 1182–1194.

Fabbiano, F., Corsi, J., Gurrieri, E., Trevisan, C., Notarangelo, M., & D'agostino, V. G. (2020). RNA packaging into extracellular vesicles: An orchestra of RNA-binding proteins? *Journal of Extracellular Vesicles*, *10*, e12043.

Finkbeiner, S. (2011). Huntington's disease. *Cold Spring Harbor Perspectives in Biology*, *3*, a007476–a007476.

Fritz, J. V., Heintz-Buschart, A., Ghosal, A., Wampach, L., Etheridge, A., Galas, D., & Wilmes, P. (2016). Sources and functions of extracellular small RNAs in human circulation. *Annual Review of Nutrition*, *36*, 301–336.

Fu, C., Chen, S., Cai, N., Liu, Z., Wang, P., & Zhao, J. (2019). Potential neuroprotective effect of miR-451 against cerebral ischemia/reperfusion injury in stroke patients and a mouse model. *World Neurosurgery*, *130*, e54–e61.

Gámez-Valero, A., Campdelacreu, J., Vilas, D., Ispierto, L., Reñé, R., Álvarez, R., Armengol, M. P., Borràs, F. E., & Beyer, K. (2019). Exploratory study on microRNA profiles from plasma-derived extracellular vesicles in Alzheimer's disease and dementia with Lewy bodies. *Translational Neurodegeneration*, *8*, 1–17.

Gámez-Valero, A., Monguió-Tortajada, M., Carreras-Planella, L., Franquesa, M. ·L., Beyer, K., & Borràs, F. E. (2016). Size-exclusion chromatography-based isolation minimally alters extracellular vesicles' characteristics compared to precipitating agents. *Scientific Reports*, *6*, 1–9.

Geekiyanage, H., Rayatpisheh, S., Wohlschlegel, J. A., Brown, R., & Ambros, V. (2020). Extracellular microRNAs in human circulation are associated with miRISC complexes that are accessible to anti-AGO2 antibody and can bind target mimic oligonucleotides. *Proceedings of the National Academy of Sciences*, *117*, 24213–24223.

Ghafouri-Fard, S., Khoshbakht, T., Hussen, B. M., Taheri, M., Ebrahimzadeh, K., & Noroozi, R. (2022). The emerging role of long non-coding RNAs, microRNAs, and an accelerated epigenetic age in Huntington's disease. *Frontiers in Aging Neuroscience*, *14*, 1–14.

Heitzer, E., Roberts, C. E. S., & Speicher, M. R. (2019). Current and future perspectives of liquid biopsies in genomics-driven oncology. *Nature Reviews Genetics*, *20*, 71–88.

Hoss, A. G., Labadorf, A., Latourelle, J. C., Kartha, V. K., Hadzi, T. C., Gusella, J. F., Macdonald, M. E., Chen, J.-F., Akbarian, S., Weng, Z., Vonsattel, J. P., & Myers, R. H. (2015). MiR-10b-5p expression in Huntington's disease brain relates to age of onset and the extent of striatal involvement. *BMC Medical Genomics*, *8*, 1–14.

Hoss, A. G., Lagomarsino, V. N., Frank, S., Hadzi, T. C., Myers, R. H., & Latourelle, J. C. (2015). Study of plasma-derived miRNAs mimic differences in Huntington's disease brain. *Movement Disorders*, *30*, 1961–1964.

Jeppesen, D. K., Fenix, A. M., Franklin, J. L., Higginbotham, J. N., Zhang, Q., Zimmerman, L. J., Liebler, D. C., Ping, J., Liu, Q., Evans, R., Fissell, W. H., Patton, J. G., Rome, L. H., Burnette, D. T., & Coffey, R. J. (2019). Reassessment of exosome composition. *Cell*, *177*, 428–445. e18.

Langfelder, P., Cantle, J. P., Chatzopoulou, D., Wang, N., Gao, F., Al-Ramahi, I., Lu, X.-H., Ramos, E. M., El-Zein, K., Zhao, Y., Deverasetty, S., Tebbe, A., Schaab, C., Lavery, D. J., Howland, D., Kwak, S., Botas, J., Aaronson, J. S., Rosinski, J., … Yang, X. W. (2016). Integrated genomics and proteomics define Huntingtin CAG length-dependent networks in mice. *Nature Neuroscience*, *19*, 623–633..

Langfelder, P., Gao, F., Wang, N., Howland, D., Kwak, S., Vogt, T. F., Aaronson, J. S., Rosinski, J., Coppola, G., Horvath, S., & Yang, X. W. (2018). MicroRNA signatures of endogenous Huntingtin CAG repeat expansion in mice. *PLoS ONE*, *13*, 1–20..

Larios, J., Mercier, V., Roux, A., & Gruenberg, J. (2020). ALIX- and ESCRT-III-dependent sorting of tetraspanins to exosomes. *Journal of Cell Biology*, *219*, e201904113.

Lässer, C., Shelke, G. V., Yeri, A., Kim, D.-K., Crescitelli, R., Raimondo, S., Sjöstrand, M., Gho, Y. S., Van Keuren Jensen, K., & Lötvall, J. (2017). Two distinct extracellular RNA signatures released by a single cell type identified by microarray and next-generation sequencing. *RNA Biology*, *14*, 58–72.

Leidinger, P., Backes, C., Deutscher, S., Schmitt, K., Mueller, S. C., Frese, K., Haas, J., Ruprecht, K., Paul, F., Stähler, C., Lang, C. J., Meder, B., Bartfai, T., Meese, E., & Keller, A. (2013). A blood based 12-miRNA signature of Alzheimer disease patients. *Genome Biology*, *14*, R78.

Love, M. I., Huber, W., & Anders, S. (2014). Moderated estimation of fold change and dispersion for RNA-seq data with DESeq2. *Genome Biology*, *15*, 1–21.

Luo, X., Jean-Toussaint, R., Sacan, A., & Ajit, S. K. (2021). Differential RNA packaging into small extracellular vesicles by neurons and astrocytes. *Cell Communication and Signaling*, *19*, 1–15.

MacDonald, M. E., Ambrose, C. M., Duyao, M. P., Myers, R. H., Lin, C., Srinidhi, L., Barnes, G., Taylor, S. A., James, M., Groot, N., MacFarlane, H., Jenkins, B., Anderson, M. A., Wexler, N. S., Gusella, J. F., Bates, G. P., Baxendale, S., Hummerich, H., Kirby, S., … Harper, P. S. (1993). A novel gene containing a trinucleotide repeat that is expanded and unstable on Huntington's disease chromosomes. *Cell*, *72*, 971–983.

Margolis, L., & Sadovsky, Y. (2019). The biology of extracellular vesicles: The known unknowns. *Plos Biology*, *17*, 1–12.

Martí, E., Pantano, L., Bañez-Coronel, M., Llorens, F., Miñones-Moyano, E., Porta, S., Sumoy, L., Ferrer, I., & Estivill, X. (2010). A myriad of miRNA variants in control and Huntington's disease brain regions detected by massively parallel sequencing. *Nucleic Acids Research*, *38*, 7219–7235.

Martí, E., Pantano, L., Bañez-Coronel, M., Llorens, F., Miñones-Moyano, E., Porta, S., Sumoy, L., Ferrer, I., & Estivill, X. (2010). A myriad of miRNA variants in control and Huntington's disease brain regions detected by massively parallel sequencing. *Nucleic Acids Research*, *38*, 7219–7235.

Martin, M. (2011). Cutadapt removes adapter sequences from high-throughput sequencing reads. *EMBnet. Journal*, *17*, 10–12.

Monguió-Tortajada, M., Morón-Font, M., Gámez-Valero, A., Carreras-Planella, L., Borràs, F. E., & Franquesa, M. (2019). Extracellular-vesicle isolation from different biological fluids by size-exclusion chromatography. *Current Protocols in Stem Cell Biology*, *49*, 1–24.

Moufarrej, M. N., Vorperian, S. K., Wong, R. J., Campos, A. A., Quaintance, C. C., Sit, R. V., Tan, M., Detweiler, A. M., Mekonen, H., Neff, N. F., Baruch-Gravett, C., Litch, J. A., Druzin, M. L., Winn, V. D., Shaw, G. M., Stevenson, D. K., & Quake, S. R. (2022). Early prediction of preeclampsia in pregnancy with cell-free RNA. *Nature*, *602*, 689–694.

Murillo, O. D., Thistlethwaite, W., Rozowsky, J., Subramanian, S. L., Lucero, R., Shah, N., Jackson, A. R., Srinivasan, S., Chung, A., Laurent, C. D., Kitchen, R. R., Galeev, T., Warrell, J., Diao, J. A., Welsh, J. A., Hanspers, K., Riutta, A., Burgstaller-Muehlbacher, S., Shah, R. V., … Milosavljevic, A. (2019). exRNA atlas analysis reveals distinct extracellular RNA cargo types and their carriers present across human biofluids. *Cell*, *177*, 463–477. e15.

Pantano, L., Estivill, X., & Martí, E. (2011). A non-biased framework for the annotation and classification of the non-miRNA small RNA transcriptome. *Bioinformatics*, *27*, 3202–3203.

Pantano, L., Friedländer, M. R., Escaramís, G., Lizano, E., Pallarès-Albanell, J., Ferrer, I., Estivill, X., & Martí, E. (2016). Specific small-RNA signatures in the amygdala at premotor and motor stages of Parkinson's disease revealed by deep sequencing analysis. *Bioinformatics*, *32*, 673–681..

Parkin, G. M., Corey-Bloom, J., Snell, C., Castleton, J., & Thomas, E. A. (2021). Plasma neurofilament light in Huntington's disease: A marker for disease onset, but not symptom progression. *Parkinsonism & Related Disorders*, *87*, 32–38.

Paulsen, J. S., Langbehn, D. R., Stout, J. C., Aylward, E., Ross, C. A., Nance, M., Guttman, M., Johnson, S., Macdonald, M., Beglinger, L. J., Duff, K., Kayson, E., Biglan, K., Shoulson, I., Oakes, D., & Hayden, M. (2008). Detection of Huntington's disease decades before diagnosis: The Predict-HD study. *Journal of Neurology, Neurosurgery, and Psychiatry*, *79*, 874–880.

Paulsen, J. S., Miller, A. C., Hayes, T., & Shaw, E. (2017). Cognitive and behavioral changes in Huntington disease before diagnosis. *Handbook of Clinical Neurology*, *144*, 69–91.

Petry, S., Keraudren, R., Nateghi, B., Loiselle, A., Pircs, K., Jakobsson, J., Sephton, C., Langlois, M., St-Amour, I., & Hébert, S. S. (2022). Widespread alterations in microRNA biogenesis in human Huntington's disease putamen. *Acta Neuropathologica Communications*, *10*, 106.

Przybyl, L., Wozna-wysocka, M., Kozlowska, E., & Fiszer, A. (2021). What, when and how to measure—Peripheral biomarkers in therapy of Huntington's disease. *International Journal of Molecular Sciences*, *22*, 1–21.

Reed, E. R., Latourelle, J. C., Bockholt, J. H., Bregu, J., Smock, J., Paulsen, J. S., Myers, R. H., De Soriano, I., Hobart, C., Miller, A., Geschwind, M. D., Sha, S., Winer, J., Satris, G., Panegyres, P., Lee, J., Tedesco, M., Maxwell, B., Perlmutter, J., … Montross, K. (2018). MicroRNAs in CSF as prodromal biomarkers for Huntington disease in the PREDICT-HD study. *Neurology*, *90*, E264–E272.

Rodrigues, F. B., Byrne, L. M., Tortelli, R., Johnson, E. B., Wijeratne, P. A., Arridge, M., De Vita, E., Ghazaleh, N., Houghton, R., Furby, H., Alexander, D. C., Tabrizi, S. J., Schobel, S., Scahill, R. I., Heslegrave, A., Zetterberg, H., & Wild, E. J. (2020). Mutant huntingtin and neurofilament light have distinct longitudinal dynamics in Huntington's disease. *Science Translational Medicine*, *12*, eabc2888.

Rozowsky, J., Kitchen, R. R., Park, J. J., Galeev, T. R., Diao, J., Warrell, J., Thistlethwaite, W., Subramanian, S. L., Milosavljevic, A., & Gerstein, M. (2019). exceRpt: A comprehensive analytic platform for extracellular RNA profiling. *Cell Systems*, *8*, 352–357. e3.

Sampedro, F., Martínez-Horta, S., Pérez-Pérez, J., Pérez-González, R., Horta-Barba, A., Campolongo, A., Izquierdo, C., Aracil-Bolaños, I., Rivas, E., Puig-Davi, A., Pagonabarraga, J., Gómez-Ansón, B., & Kulisevsky, J. (2022). Plasma TDP-43 reflects cortical neurodegeneration and correlates with neuropsychiatric symptoms in Huntington's disease. *Clinical Neuroradiology*, *32*, 1077–1085.

Scahill, R. I., Zeun, P., Osborne-Crowley, K., Johnson, E. B., Gregory, S., Parker, C., Lowe, J., Nair, A., O'callaghan, C., Langley, C., Papoutsi, M., Mccolgan, P., Estevez-Fraga, C., Fayer, K., Wellington, H., Rodrigues, F. B., Byrne, L. M., Heselgrave, A., Hyare, H., … Tabrizi, S. J. (2020). Biological and clinical characteristics of gene carriers far from predicted onset in the Huntington's disease Young Adult Study (HD-YAS): A cross-sectional analysis. *Lancet Neurology*, *19*, 502–512.

Schageman, J., Zeringer, E., Li, M., Barta, T., Lea, K., Gu, J., Magdaleno, S., Setterquist, R., & Vlassov, A. V. (2013). The complete exosome workflow solution: From isolation to characterization of RNA cargo. *BioMed Research International*, *2013*, 6.

Schobel, S. A., Palermo, G., Auinger, P., Long, J. D., Ma, S., Khwaja, O. S., Trundell, D., Cudkowicz, M., Hersch, S., Sampaio, C., Dorsey, E. R., Leavitt, B. R., Kieburtz, K. D., Sevigny, J. J., Langbehn, D. R., Tabrizi, S. J., Adams, J., Jog, M., Hyson, C., … Campbell, C. (2017). Motor, cognitive, and functional declines contribute to a single progressive factor in early HD. *Neurology*, *89*, 2495–2502.

Sheinerman, K. S., Tsivinsky, V. G., Crawford, F., Mullan, M. J., Abdullah, L., & Umansky, S. R. (2012). Plasma microRNA biomarkers for detection of mild cognitive impairment. *Aging*, *4*(9), 590–605. https://doi.org/10.18632/aging.100486

Shi, J., Zhang, Y., Tan, D., Zhang, X., Yan, M., Zhang, Y., Franklin, R., Shahbazi, M., Mackinlay, K., Liu, S., Kuhle, B., James, E. R., Zhang, L., Qu, Y., Zhai, Q., Zhao, W., Zhao, L., Zhou, C., Gu, W., … Chen, Q. (2021). PANDORA-seq expands the repertoire of regulatory small RNAs by overcoming RNA modifications. *Nature Cell Biology*, *23*, 424–436..

Southwell, A. L., Smith, S. E. P., Davis, T. R., Caron, N. S., Villanueva, E. B., Xie, Y., Collins, J. A., Ye, M. L., Sturrock, A., Leavitt, B. R., Schrum, A. G., & Hayden, M. R. (2015). Ultrasensitive measurement of huntingtin protein in cerebrospinal fluid demonstrates increase with Huntington disease stage and decrease following brain huntingtin suppression. *Scientific Reports*, *5*, 1–11.

Srinivasan, S., Yeri, A., Cheah, P. S., Chung, A., Danielson, K., De Hoff, P., Filant, J., Laurent, C. D., Laurent, L. D., Magee, R., Moeller, C., Murthy, V. L., Nejad, P., Paul, A., Rigoutsos, I., Rodosthenous, R., Shah, R. V., Simonson, B., To, C., … Laurent, L. C. (2019). Small RNA sequencing across diverse biofluids identifies optimal methods for exRNA isolation. *Cell*, *177*, 446–462.e16.

Tabrizi, S. J., Flower, M. D., Ross, C. A., & Wild, E. J. (2020). Huntington disease: New insights into molecular pathogenesis and therapeutic opportunities. *Nature Reviews Neurology*, *16*, 529–546.

Tabrizi, S. J., Ghosh, R., & Leavitt, B. R. (2019). Huntingtin lowering strategies for disease modification in Huntington's disease. *Neuron*, *101*, 801–819.

Tabrizi, S. J., Schobel, S., Gantman, E. C., Mansbach, A., Borowsky, B., Konstantinova, P., Mestre, T. A., Panagoulias, J., Ross, C. A., Zauderer, M., Mullin, A. P., Romero, K., Sivakumaran, S., Turner, E. C., Long, J. D., & Sampaio, C. (2022). A biological classification of Huntington's disease: The integrated staging system. *Lancet Neurology*, *21*, 632–644.

Tan, L., Yu, J.-T., Liu, Q.-Y., Tan, M.-S., Zhang, W., Hu, N., Wang, Y.-L., Sun, L., Jiang, T., & Tan, L. (2014). Circulating miR-125b as a biomarker of Alzheimer's disease. *Journal of the Neurological Sciences*, *336*, 52–56.

Théry, C., Witwer, K. W., Aikawa, E., Alcaraz, M. J., Anderson, J. D., Andriantsitohaina, R., Antoniou, A., Arab, T., Archer, F., Atkin-Smith, G. K., Ayre, D. C., Bach, J. M., Bachurski, D., Baharvand, H., Balaj, L., Baldacchino, S., Bauer, N. N., Baxter, A. A., Bebawy, M., … Zuba-Surma, E. K. (2018). Minimal information for studies of extracellular vesicles 2018 (MISEV2018): A position statement of the International Society for Extracellular Vesicles and update of the MISEV2014 guidelines. *119*.

Thompson, D. M., Lu, C., Green, P. J., & Parker, R. (2008). tRNA cleavage is a conserved response to oxidative stress in eukaryotes. *RNA*, *14*, 2095–2103.

Tosar, J. P., & Cayota, A. (2020). Extracellular tRNAs and tRNA-derived fragments. *RNA Biology*, *17*, 1149–1167.

Tosar, J. P., Gambaro, F., Sanguinetti, J., Bonilla, B., Witwer, K. W., & Cayota, A. (2015). Assessment of small RNA sorting into different extracellular fractions revealed by high-throughput sequencing of breast cell lines. *Nucleic Acids Research*, *43*, 5601–5616.

Tosar, J. P., Segovia, M., Castellano, M., Gámbaro, F., Akiyama, Y., Fagúndez, P., Olivera, Á., Costa, B., Possi, T., Hill, M., Ivanov, P., & Cayota, A. (2020). Fragmentation of extracellular ribosomes and tRNAs shapes the extracellular RNAome. *Nucleic Acids Research*, *48*, 12874–12888.

Van Deun, J., Mestdagh, P., Agostinis, P., Akay, Ö., Anand, S., Anckaert, J., Martinez, Z. A., Baetens, T., Beghein, E., Bertier, L., Berx, G., Boere, J., Boukouris, S., Bremer, M., Buschmann, D., Byrd, J. B., Casert, C., Cheng, L., Cmoch, A., … Hendrix, A. (2017). EV-TRACK: Transparent reporting and centralizing knowledge in extracellular vesicle research. *Nature Methods*, *14*, 228–232.

Vickers, K. C., Palmisano, B. T., Shoucri, B. M., Shamburek, R. D., & Remaley, A. T. (2011). MicroRNAs are transported in plasma and delivered to recipient cells by high-density lipoproteins. *Nature Cell Biology*, *13*, 423–433.

Wang, H. (2023). MicroRNA pathological mechanisms between Parkinson's disease, Alzheimer's disease, glaucoma and macular degeneration. *Expert Reviews in Molecular Medicine*, *25*, e24. https://doi.org/10.1017/erm.2023.19

Wang, X., Hong, Y., Wu, L., Duan, X., Hu, Y., Sun, Y., Wei, Y., Dong, Z., Wu, C., Yu, D., & Xu, J. (2021). Deletion of microRNA-144/451 cluster aggravated brain injury in intracerebral hemorrhage mice by targeting 14-3-3ζ. *Frontiers in Neurology*, *11*, 551411.

Weir, D. W., Sturrock, A., & Leavitt, B. R. (2011). Development of biomarkers for Huntington's disease. *Lancet Neurology*, *10*, 573–590.

Wild, E. J., Boggio, R., Langbehn, D., Robertson, N., Haider, S., Miller, J. R. C., Zetterberg, H., Leavitt, B. R., Kuhn, R., Tabrizi, S. J., Macdonald, D., & Weiss, A. (2015). Quantification of mutant huntingtin protein in cerebrospinal fluid from Huntington's disease patients. *Journal of Clinical Investigation*, *125*, 1979–1986.

Yeri, A., Courtright, A., Reiman, R., Carlson, E., Beecroft, T., Janss, A., Siniard, A., Richholt, R., Balak, C., Rozowsky, J., Kitchen, R., Hutchins, E., Winarta, J., Mccoy, R., Anastasi, M., Kim, S., Huentelman, M., & Van Keuren-Jensen, K. (2017). Total extracellular small RNA profiles from plasma, saliva, and urine of healthy subjects. *Scientific Reports*, *7*, 1–13.

SUPPORTING INFORMATION

Additional supporting information can be found online in the Supporting Information section at the end of this article.

How to cite this article: Herrero-Lorenzo, M., Pérez-Pérez, J., Escaramís, G., Martínez-Horta, S., Pérez-González, R., Rivas-Asensio, E., Kulisevsky, J., Gámez-Valero, A., & Martí, E. (2024). Small RNAs in plasma extracellular vesicles define biomarkers of premanifest changes in Huntington's disease. *Journal of Extracellular Vesicles*, *13*, e12522. https://doi.org/10.1002/jev2.12522